Selection of the Optimum Frequency Channels of Microwave Radiometers for Upcoming Radar Altimetry Missions

Jose Mª Gual de Torrella Covas

Director: Adriano Camps Carmona

Escola Tècnica Superior de Telecomunicacions de Barcelona

Universitat Politècnica de Catalunya

CONTENTS

List of Figures

LIST OF TABLES

SUMMARY

Nowadays, radar altimetry measurements provide us very important data related to weather, climate etc. However, the current technology has a lot of limitations, for example, the resolution of height measurements (vertical resolution) is not as good as required or data close to the coast is not reliable. This type of resolution must be as accurate as it can, because, for example, a variation of cm of order on the sea level can means very big changes around the Earth. This lack of resolution is related, among other factors to the down looking brightness temperatures measured by the companion microwave radiometers in charge of the wet delay correction.

New technologies and methods can now be applied to radar altimetry to improve the spatial resolution and get closer to the coast. Therefore, it is necessary to improve or find better ways to measure accurately the brightness temperature close to the coastline.

CHAPTER 1

INTRODUCTION

Satellite altimetry plays an import an role in Earth observation techniques, and it is very useful for ocean missions. *Coastal Altimetry* (approximately 0-50 km away from the coast) allows to study storm surge's by measuring the Total Water Level Envelope (TWLE), and is also very useful to define wave models. However, coastal altimetry data is inaccurate and difficult to interpret due to the variation on the waveforms' shape (shape of the radar returns) when the antenna footprint of the instrument enters in the land, and because of the rapid variation of the wet tropospheric delay. The application of SAR techniques to radar altimetry, such as in ESA's CryoSat-2 mission has allowed to significantly improve the along-track resolution, providing much better results than in pulse-limited altimeters [3]. Nevertheless for these altimeters, an optimized delay correction is needed to solve the rapid tropospheric wet delay variability [2]. In this study, a methodology is presented to identify from the measured brightness temperatures on top of the atmosphere, a set of frequency channels that provide the most significant and uncorrelated information on the water vapor content in the atmosphere . First of all, a mathematical model is defined to describe the Physics of the atmosphere, and from this model the contribution of the water vapor into the brightness temperatures as measured by a spaceborne nadir-looking microwave radiometer is derived. Then, four different mathematical models to select the frequency channels providing the largest amount of data (i.e. uncorrelated data) are presented, and electrical path delay accuracy method is derived. For the three "standard" cli-

mates (temperate, tropical and polar) with the four proposed methods are evaluated and compared along the information provided and the reached electrical path delay accuracy. Synthetic atmospheric pressure, temperature, and water vapor profiles by considering different surface emissivities, are used in the computation of the down-looking brightness temperatures for the three types of atmosphere.

Finally, from the selected method, it is evaluated the accuracy of the excess electrical path delay accuracy when there is presence of noise in the channels selected.

1.1 Satellite Altimetry: Principles

Satellite altimetry determines the altitude (altimeter range) of the satellite above the surface by sending a radar pulse towards the surface (sea or land surface) and measuring the time needed for the pulse to come back to its generator (the satellite). Using the estimated altitude (altimeter range), and knowing the orbit heigh of the satellite, it can be calculated the sea or land surface [2], [4].

Altimetric measurement require a high precision (few cm) from a satellite orbiting at around $500-1000$ km over the surface. For this accuracy a precise knowledge of satellite's orbital position is needed, which is achieved through the use of several positioning systems. Also it is needed to apply corrections in the altimetry calculations caused by electrons in the ionosphere, and to gases and water vapor.

An interesting application of this field is the *Oceanic* and *Coastal Altimetry*, that as explained previously, allows to study storm surge's and define wave models. Figure 1.1 shows an schematic of an oceanic radar altimeter with all distances that used in this technique [1].

As it can be observed in this figure, the dynamic change of the sea surface elevation must be taken into consideration when altimetry is measured in oceanic and coastal surfaces. Concepts of dynamic topography (DT) are introduced.

The geoid is the sea surface in an instant and in an precise location caused by the currents during the time. Knowing the constant sea surface (average), the dynamic topography (DT) is calculated as the its difference with respect to the geoid. At the same time, the mean sea surface is got from the radar pulse sent by the satellite altimetry, as the difference between the satellite orbit (known) and the range (measured).

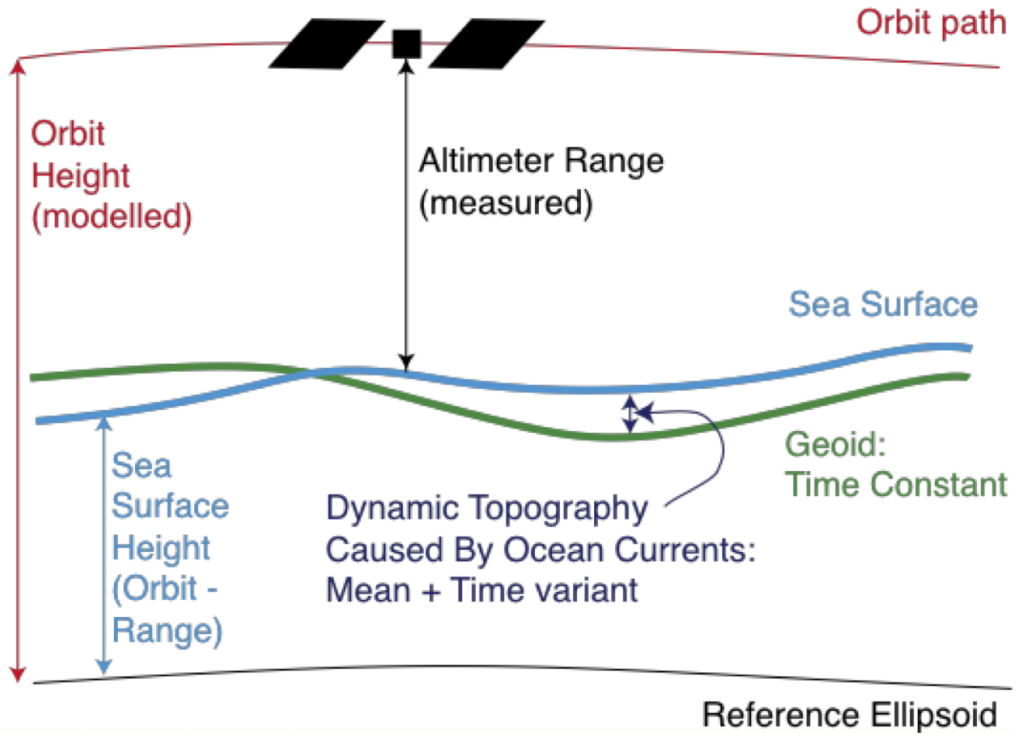

Figure 1.1: Altimetric distances [1]

1.2 The Coastal Altimetry issue

This section explains in detail the two main problems presented at the beginning of this chapter, that are faced by *Coastal Altimetry*: the change of the altimetry echoes when the satellite antenna footprint enters into the land, and the inaccuracy in the data retrieved when it is processed.

1.2.1 Altimetry echoes in coastal zones

The first problem explained and illustrated in Fig. 1.2 affects to the so-called *re-tracking* process of the normal satellite altimeters, that consists on fitting a waveform model to the waveforms and extracting the parameters from it.

Different factors are involved: on one hand the smaller beam filling factor of the ocean surface, and on the other hand, the surface topography of the beam filled by the land surface.

Techniques to improve the so-called *re-tracking* process are presented as a solution for this problem within the framework of the international coastal altimetry community (e.g. COASTAL

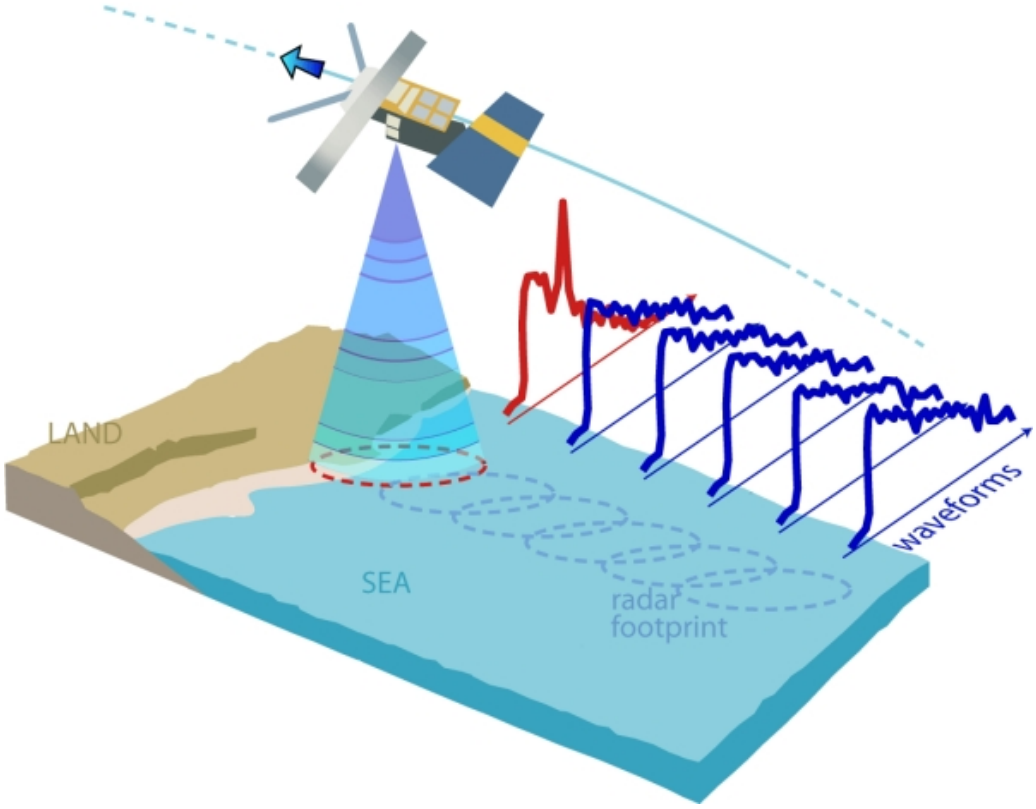

Figure 1.2: Waveform changing when altimeter enters into the land [2]

and PISTACH projects, [2], [5]). The basis of these techniques consists of combining previous and following waveforms information retrieved from the surface. This is possible through the Synthetic Aperture Radar (SAR) altimetry. This technique utilizes the flight path of the platform to simulate a very large antenna or aperture electronically, that generates a high-resolution image. For each position of the antenna, a radar pulse is transmitted, that is recovered back by the receiver and recorded, and combined with previous and following pulses to form the synthetic aperture. Figure 1.3 presents the logic of the SAR data processing where, by order, it is applied in first term the along-track FFTS (Doppler shift) to the digitalized pulses, then the range curvature correction (delay shift), and the range curve compression (common with pulse-limited altimeters). All this processed information is allocated in memory to then be combined at each Doppler and look (multi-look).

The achieved effect is similar to that of a phased array, but using only a unique antenna, increasing the gain and improving the resolution with respect to the pulse-limited footprint radars.

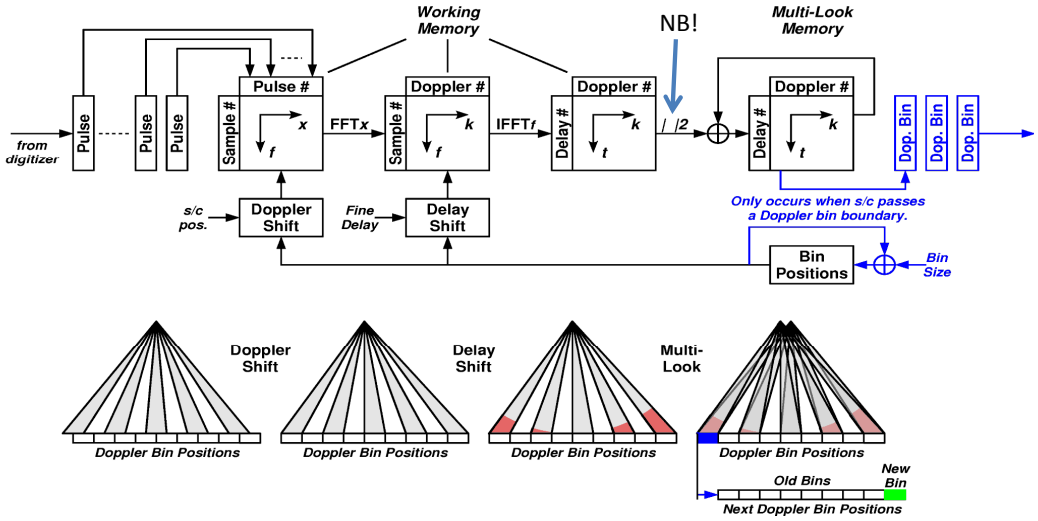

Figure 1.3: SAR waveform processing [1]

1.2.2 Data processing accuracy

The second issue presented concerns to the accuracy during data processing affected by the atmospheric components in coastal zones. In these zones, the most critical corrections are the ones due to the ocean tides, water vapor, and the sea state bias (SSB) [2].

The case of study of this project is the inaccurate correction of the path delay due to water vapor, named *wet tropospheric correction*. Wet tropospheric correction is normally estimated by using a multi-channel passive microwave radiometer from the same platform as the altimeter. This data becomes useless once the radiometer foot print enters in the land ($\sim 20-50$ km from the coast). Different solutions to this issue are available. This project focuses in the improvement of the estimation of water vapor content in the atmosphere, by selecting the optimum microwave channels.

CHAPTER 2

SELECTION OF THE OPTIMUM FREQUENCY CHANNELS

The objective of this project is to find a the optimum set of channels (frequencies) to measure the atmospheric water vapor content and its variability to perform the corrections to the range measurements of upcoming SAR radiometry altimeters. These channels will be selected by using the weighting functions of the brightness temperatures measured by spaceborne radiometers, which include the contributions of the emitted atmospheric radiation, the atmospheric radiation reflected in the Earth's surface back to the space, and the radiation of the Earth's surface.

In this chapter, the methodology used in this project to achieve the final results is explained. First, a mathematical model from the Physics of the Radiative Transfer Model that define the measured brightness temperature (*forward-model*) is described. This model is used to calculate the weighting functions of the brightness temperatures [6], and then, using Inverse Methods [7] based on the Information Content of each frequency (channel), to iteratively select the number of optimum frequencies to measure the atmospheric water vapor in the troposphere is selected iteratively.

2.1 Forward Model

As explained in Chapter 1, in this project three different atmospheric profiles are considered for the three different climates: tropical, temperate, and polar, and for three different types of surfaces: ice, sea, and coast. The three standard atmosphere models are generated using as input parameters the surface water vapor, the temperature, and the pressure, from 0 km (sea surface height) to 64 km height (mesosphere). The atmospheric temperature, pressure, and water vapor profiles ($T(z)$, $P(z)$, and $\rho_v(z)$ Figs. 2.1, 2.2, and 2.3) for the three different climates are described in [8], and they are used to compute the gas absorption κ_α, the atmospheric optical thickness $\tau(z,\infty)$ (Eqn. 2.1 , the upwelling temperature, and the downwelling temperature as a function of the frequency (f). Finally, three different surface emissivities are used to calculate the surface brightness temperatures (T_b), and the atmospheric downwelling temperature reflected back to the atmosphere (T_{SC} Eqn. 2.5) (Fig. 2.4).

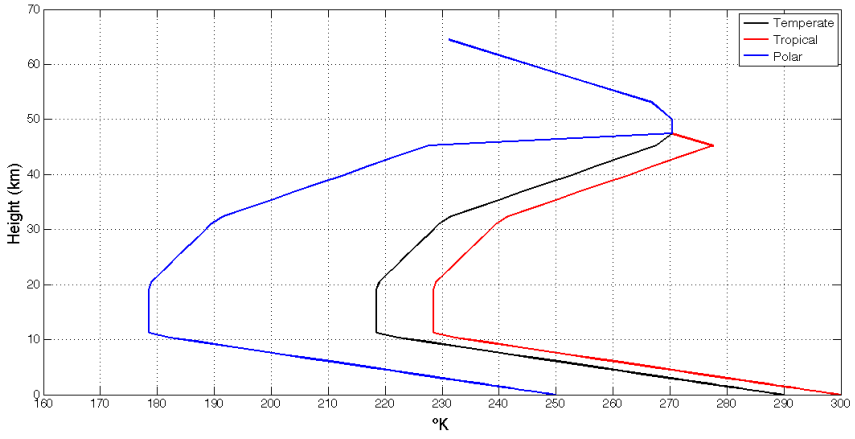

Figure 2.1: Temperature Profiles

$$\tau(z,\infty) = \tau_0 \cdot sec(\theta) = \int_0^\infty k_\alpha(f,z)dz \cdot sec(\theta). \tag{2.1}$$

The emissivity values are 1.00, 0.50, and 0.75, which correspond approximately to those of the ice, oceans and coastal regions (50% ocean, 50% land), respectively. Finally, the brightness temperature reaching the radiometer antenna (T_B, Eqn. 2.2) is then computed for the nine possible combinations of the three different climates and the three different surfaces:

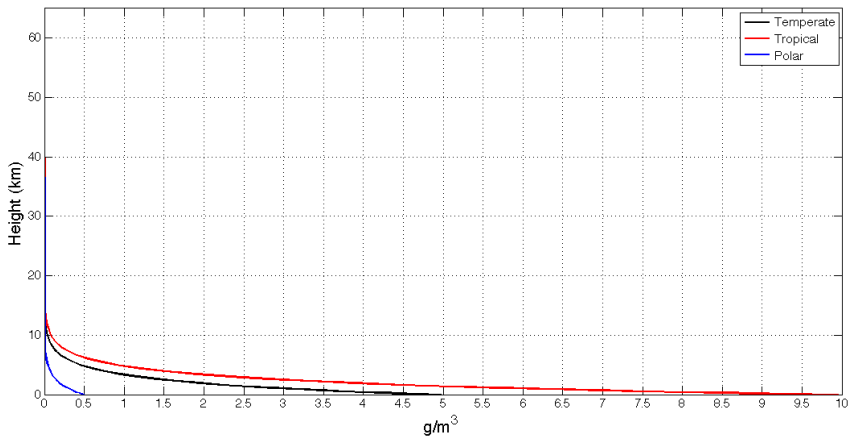

Figure 2.2: Water Vapor Profiles

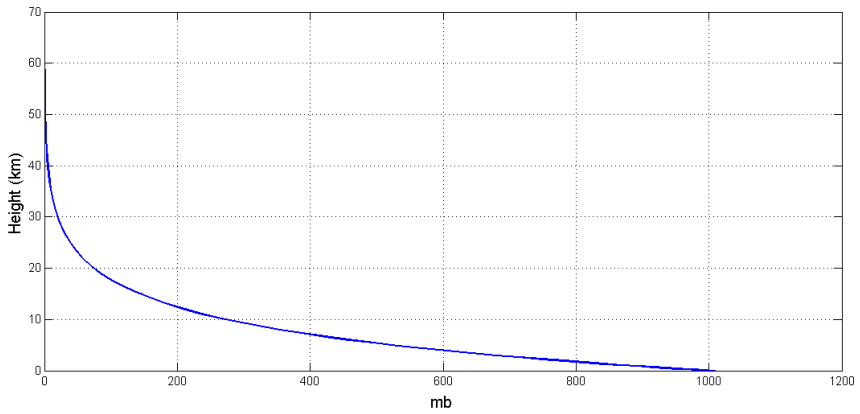

Figure 2.3: Pressure Profile

$$T_B(\theta) = T_{UP} + T_b + T_{SC}, \tag{2.2}$$

$$T_{UP} = sec(\theta) \cdot \int_0^{\infty} \kappa_\alpha(f,z) \cdot T(z) \cdot e^{-\tau(z,\infty)}, \cdot dz, \tag{2.3}$$

$$T_b = e_s \cdot T_s \cdot e^{-\tau(0,\infty)}, \tag{2.4}$$

$$T_{SC} = (1-e_s) \cdot sec(\theta) \cdot \int_{\infty}^{0} \kappa_\alpha(f,z) \cdot T(z) \cdot e^{-\tau(0,z)} \cdot dz, \tag{2.5}$$

where each contribution to the brightness temperature is represented in the Fig. 2.4. The nadir-looking brightness temperature T_B (Eqn. 2.6) can also be written as Eqn. 2.6

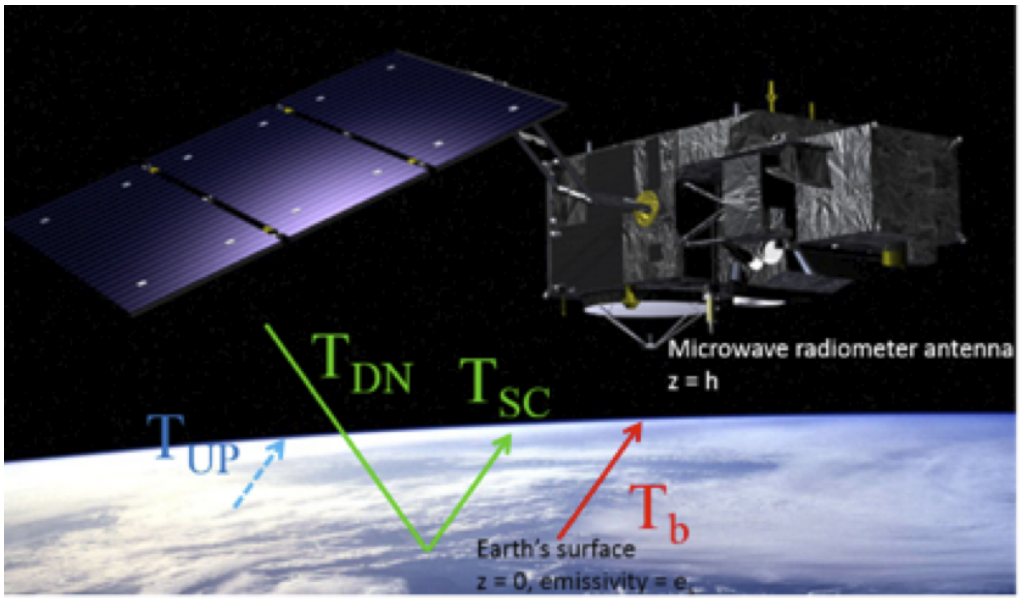

Figure 2.4: Schematic observation brightness temperatures

In Eqns. 2.4 and 2.5, e_s and T_s are the surface's emissivity temperature, and θ is the zenit angle. The brightness temperature reaching the radiometer (T_B) can also be written as:

$$T_B(\theta) = sec(\theta) \cdot \int_0^{\infty} \rho_v(f,z) \cdot K_W^{\uparrow}(f,\theta,z) \cdot dz, \tag{2.6}$$

where $K_W^{\uparrow}$ is the so-called water vapor weighting function, which indicates the contribution of the atmospheric water vapor content at height z, to the measured brightness temperature (T_B) at a frequency f, under an observation angle θ ($\theta = 0°$ at nadir) and, over surface of emissivity e_s [6]. The water vapor weighting function is calculated as the derivative of the brightness temperature with respect to the water vapor profile:

$$\begin{aligned} K_W^{\uparrow}(f,\theta,z) = & \frac{\delta\kappa_{alpha}(f,T,\rho_v)}{\delta_{\rho_v}} \cdot sec(\theta) \cdot \\ & \cdot e^{-\tau(z,h)} \cdot \left\{ -[(1-e_s) \cdot T_{DN} + e_s \cdot T_s] \cdot e^{-\tau(0,z)} - \int_0^z T(z') \cdot \kappa_\alpha(f,T,\rho_v) \cdot sec(\theta) \cdot e^{-\tau(z',z)} \cdot dz' \right\} + \\ & + K_W^{\downarrow}(f,\theta,z), \end{aligned} \tag{2.7}$$

where T_s is the temperature at the surface level ($z = 0$), T_{DN} is the downwelling temperature emitted by the atmosphere, and $K_W^{\downarrow}(f,\theta,z)$ is the water vapor weighting function for an upward looking radiometer (Eqn. 2.8):

$$K_W^{\downarrow} = \frac{\delta\kappa_\alpha(f,T,\rho_v}{\delta\rho_v} \cdot sec(\theta) \cdot \left\{ -\int_z^h T(z') \cdot \kappa_\alpha(f,T,\rho_v) \cdot sec(\theta) \cdot e^{-\tau(z,z')} \cdot dz' \right\}. \tag{2.8}$$

From Eqn. 2.7 the sensibility of the observation (frequency channel) to the atmospheric water vapor variations, can be analyzed as well as the impact of different surfaces (ice, ocean, and coastal).

2.2 Model linearization

The forward model presented in Eqns. 2.2 and 2.6 can be discretized in order to facilitate the calculation using algebraic methods [7]. This discrete model is presented below, where the bold symbols indicate vectors (lower case) and matrices (upper case).

$$\hat{\boldsymbol{y}} = \boldsymbol{K_W} \cdot \boldsymbol{x} + \boldsymbol{\varepsilon}. \tag{2.9}$$

In this discrete model the brightness temperature observations (T_B) are represented by the vector $\hat{\boldsymbol{y}}$, whose dimension corresponds to the number of observation channels (frequency channels) to be analyzed. The unknown profile information (ρ_v in this project) along the atmospheric height z is $\boldsymbol{x}$, the error of each observation caused by the instruments' calibration errors and the noise is $\boldsymbol{\varepsilon}$, and the contribution of each atmospheric profile component per height and frequency to the brightness temperature is given by the matrix $\boldsymbol{K_W}$. The weighting function matrix $\boldsymbol{K_W}$ will be of $m \cdot n$ dimensions, where there is a contribution into the brightness temperature at each frequency channel (m channels) from each height (n layers). Equation 2.10 shows in detail the discrete forward model presented in Eqn. 2.9, where each position n of the vector $\hat{\boldsymbol{y}}$ corresponds to an observation on the frequency channel f_n, each position m of the vector $\boldsymbol{x}$ corresponds to the atmospheric profile on the height h_m, and the weighting function matrix $\boldsymbol{K_W}$ is a linear combination of both height and frequency which contains the contribution or *weight* of the atmospheric profile $\boldsymbol{x}$ to the space of measured brightness temperature $\hat{\boldsymbol{y}}$.

$$\begin{pmatrix} y(f_1) \\ y(f_2) \\ y(f_3) \\ \vdots \\ y(f_M) \end{pmatrix} = \begin{pmatrix} K_{1,1} & K_{1,2} & K_{1,3} & \cdots & K_{1,N} \\ K_{2,1} & K_{2,2} & K_{2,3} & \cdots & K_{2,N} \\ K_{3,1} & K_{3,2} & K_{3,3} & \cdots & K_{3,N} \\ \vdots & \vdots & \vdots & \ddots & \vdots \\ K_{M,1} & K_{M,2} & K_{M,3} & \cdots & K_{M,N} \end{pmatrix} \cdot \begin{pmatrix} x(h_1) \\ x(h_2) \\ x(h_3) \\ \vdots \\ x(h_N) \end{pmatrix}. \tag{2.10}$$

The number of height levels (n) is 60 between 0 and 64 km in steps of 0.1 to 0.8 km for the troposphere, 0.8 km to 2 km for the stratosphere, and 2 km to 4 km for the mesosphere. A total number of channels (m) around the water vapor resonance frequencies are analyzed in steps of 100 MHz.

The probability density function of the measurements and the state space $P(\hat{\boldsymbol{y}})$ and $P(\boldsymbol{x})$ are assumed as Gaussians with a zero-mean experimental error (Eqns. 2.11 and 2.12)

$$P(\boldsymbol{y}) = \frac{1}{(2\pi)^{n/2} \cdot |\boldsymbol{S_y}|^{1/2}} \cdot e^{-\frac{1}{2} \cdot (\boldsymbol{y}-\boldsymbol{E(y)}) \cdot \boldsymbol{S_y^{-1}} \cdot (\boldsymbol{y}-\boldsymbol{E(y)})}, \tag{2.11}$$

$$P(\boldsymbol{x}) = \frac{1}{(2\pi)^{n/2} \cdot |\boldsymbol{S_a}|^{1/2}} \cdot e^{-\frac{1}{2} \cdot (\boldsymbol{x}-\boldsymbol{x_a}) \cdot \boldsymbol{S_a^{-1}} \cdot (\boldsymbol{x}-\boldsymbol{x_a})}, \tag{2.12}$$

where the matrices $\boldsymbol{S_y}$ and $\boldsymbol{S_a}$ are the covariance matrices of $\hat{\boldsymbol{y}}$ and $\boldsymbol{x_a}$, respectively, and the subscript a denotes the *a priori* knowledge coming from historical information of the atmosphere or from generated virtual measurements as in this study.

Bayes' theorem is used in Eqns. 2.13 and 2.14 to relate the probability density function of the observation with the one of the atmospheric state as shown:

$$P(\hat{\boldsymbol{y}}|\boldsymbol{x}) = \frac{P(\boldsymbol{x}, \boldsymbol{y})}{\int P(\boldsymbol{x}, \hat{\boldsymbol{y}})}, \tag{2.13}$$

$$P(\boldsymbol{x}|\hat{\boldsymbol{y}}) = \frac{P(\hat{\boldsymbol{y}}|\boldsymbol{x}) \cdot P(\boldsymbol{x})}{P(\hat{\boldsymbol{y}})}. \tag{2.14}$$

Then from Eqn. 2.11, Eqn. 2.13 can be written as:

$$-2 \ln P(\hat{\boldsymbol{y}}|\boldsymbol{x}) = (\hat{\boldsymbol{y}} - \boldsymbol{K_W} \cdot \boldsymbol{x})^{\boldsymbol{T}} \cdot \boldsymbol{S_\epsilon^{-1}} \cdot (\hat{\boldsymbol{y}} - \boldsymbol{K_W} \cdot \boldsymbol{x}) + c_1, \tag{2.15}$$

where $\boldsymbol{c_1}$ is the probability density function constant defined as $-\ln(2 \cdot \pi^{n/2} \cdot |\boldsymbol{S_y}|^{1/2})$.

In the same way, from Eqn. 2.12:

$$-2\ln P(\boldsymbol{x}) = (\boldsymbol{x}-\boldsymbol{x_a})^T \cdot \boldsymbol{S_a^{-1}} \cdot (\boldsymbol{x}-\boldsymbol{x_a}) + c_2, \tag{2.16}$$

where $\boldsymbol{c_2}$ is also the probability density function constant defined as $\ln(2\cdot\pi^{n/2}\cdot|\boldsymbol{S_a}|^{1/2})$.

The probability density function of the state vector improved by the brightness temperature observations (Eqn. 2.14), is expressed as Eqn. 2.17 by combining Eqn. 2.15 (in orange color) and Eqn. 2.16 (in red color):

$$-2\ln P(\boldsymbol{x}|\hat{\boldsymbol{y}}) = (\hat{\boldsymbol{y}}-\boldsymbol{K_W}\cdot\boldsymbol{x})^T \cdot \boldsymbol{S_\epsilon^{-1}} \cdot (\hat{\boldsymbol{y}}-\boldsymbol{K_W}\cdot\boldsymbol{x}) + (\boldsymbol{x}-\boldsymbol{x_a})^T \cdot \boldsymbol{S_a^{-1}} \cdot (\boldsymbol{x}-\boldsymbol{x_a}) + \boldsymbol{c_3}, \tag{2.17}$$

where the probability density function constant $\boldsymbol{c_3}$ is the sum of both constants $\boldsymbol{c_1}$ and $\boldsymbol{c_2}$.

Equation 2.17 can be written as Eqn. 2.18, where $\hat{\boldsymbol{x}}$ is the expected value of $P(\boldsymbol{x}|\hat{\boldsymbol{y}})$ and $\hat{\boldsymbol{S}}$ is its covariance matrix (Eqn. 2.18):

$$-2\ln P(\boldsymbol{x}|\hat{\boldsymbol{y}}) = (\boldsymbol{x}-\hat{\boldsymbol{x}})^T \cdot \boldsymbol{\hat{S}^{-1}} \cdot (\boldsymbol{x}-\hat{\boldsymbol{x}}) + \boldsymbol{c_4}, \tag{2.18}$$

that equating quadratic terms on $\boldsymbol{x}$ from Eqns. 2.17 and 2.18 results in:

$$\boldsymbol{x}^T \cdot \boldsymbol{K_W^T} \cdot \boldsymbol{S_\epsilon^{-1}} \cdot \boldsymbol{K_W} \cdot \boldsymbol{x} + \boldsymbol{x}^T \cdot \boldsymbol{S_a^{-1}} \cdot \boldsymbol{x} = \boldsymbol{x}^T \cdot \boldsymbol{\hat{S}^{-1}} \cdot \boldsymbol{x}, \tag{2.19}$$

gives

$$\boldsymbol{\hat{S}^{-1}} = \boldsymbol{K_W^T} \cdot \boldsymbol{S_\epsilon^{-1}} \cdot \boldsymbol{K_W} + \boldsymbol{S_a^{-1}}. \tag{2.20}$$

Likewise, equating the terms that are linear in $\boldsymbol{x}^T$ from Eqns. 2.17 and 2.18 results in:

$$(-\boldsymbol{K_W}\cdot\boldsymbol{x})^T \cdot \boldsymbol{S_\epsilon^{-1}} \cdot \hat{\boldsymbol{y}} + \boldsymbol{x}^T \cdot \boldsymbol{S_a^{-1}} \cdot (-\boldsymbol{x_a}) = \boldsymbol{x}^T \cdot \boldsymbol{\hat{S}^{-1}} \cdot (-\hat{\boldsymbol{x}}). \tag{2.21}$$

For Eqn. 2.21 only linear terms in $\boldsymbol{x}^T$ have been considered for convenience, as equating terms in $\boldsymbol{x}$ gives the transpose of this equation.

Considering that Eqn. 2.21 should be valid for any value of $\boldsymbol{x}$, then $\boldsymbol{x}^T$ can be cancelled ($\boldsymbol{x}^T = \boldsymbol{I}$) giving:

$$\boldsymbol{K}^T \cdot \boldsymbol{S_\epsilon^{-1}} \cdot \boldsymbol{y} + \boldsymbol{S_a^{-1}} \cdot \boldsymbol{x_a} = (\boldsymbol{K}^T \cdot \boldsymbol{S_\epsilon^{-1}} \cdot \boldsymbol{K} + \boldsymbol{S_a^{-1}}) \cdot \hat{\boldsymbol{x}}. \tag{2.22}$$

Thus, from Eqn. 2.20, the recovered state vector $\hat{\boldsymbol{x}}$ is presented as in Eqn. 2.23

$$\begin{aligned}\hat{\boldsymbol{x}} &= (\boldsymbol{K}_{\boldsymbol{W}}^{\boldsymbol{T}} \cdot \boldsymbol{S}_{\boldsymbol{\epsilon}}^{-\mathbf{1}} \cdot \boldsymbol{K}_{\boldsymbol{W}} + \boldsymbol{S}_{\boldsymbol{a}}^{-\mathbf{1}})^{-\mathbf{1}} \cdot (\boldsymbol{K}_{\boldsymbol{W}}^{\boldsymbol{T}} \cdot \boldsymbol{S}_{\boldsymbol{\epsilon}}^{-\mathbf{1}} \cdot \hat{\boldsymbol{y}} + \boldsymbol{S}_{\boldsymbol{a}}^{-\mathbf{1}} \cdot \boldsymbol{x}_{\boldsymbol{a}}) = \\ &= \boldsymbol{x}_{\boldsymbol{a}} + (\boldsymbol{K}_{\boldsymbol{W}}^{\boldsymbol{T}} \cdot \boldsymbol{S}_{\boldsymbol{\epsilon}}^{-\mathbf{1}} \cdot \boldsymbol{K}_{\boldsymbol{W}} + \boldsymbol{S}_{\boldsymbol{a}}^{-\mathbf{1}})^{-\mathbf{1}} \cdot \boldsymbol{K}_{\boldsymbol{W}}^{\boldsymbol{T}} \cdot \boldsymbol{S}_{\boldsymbol{\epsilon}}^{-\mathbf{1}} \cdot (\boldsymbol{y} - \boldsymbol{K}_{\boldsymbol{W}} \cdot \boldsymbol{x}_{\boldsymbol{a}}),\end{aligned} \tag{2.23}$$

that can be written as Eqn. 2.24

$$\hat{\boldsymbol{x}} = \boldsymbol{x}_{\boldsymbol{a}} + \boldsymbol{G} \cdot (\hat{\boldsymbol{y}} - \boldsymbol{K}_{\boldsymbol{W}} \cdot \boldsymbol{x}_{\boldsymbol{a}}), \tag{2.24}$$

where $\boldsymbol{G}$ denotes the contribution matrix or gain matrix defined as $(\boldsymbol{K}_{\boldsymbol{W}}^{\boldsymbol{T}} \cdot \boldsymbol{S}_{\boldsymbol{\epsilon}}^{-\mathbf{1}} \cdot \boldsymbol{K}_{\boldsymbol{W}} + \boldsymbol{S}_{\boldsymbol{a}}^{-\mathbf{1}})^{-\mathbf{1}} \cdot \boldsymbol{K}_{\boldsymbol{W}}^{\boldsymbol{T}} \cdot \boldsymbol{S}_{\boldsymbol{\epsilon}}^{-\mathbf{1}}$. In Eqn. 2.25 the so-called Averaging Kernel:

$$\begin{aligned}\boldsymbol{AK} &= \boldsymbol{S}_{\boldsymbol{a}} \cdot \boldsymbol{K}_{\boldsymbol{W}}^{\boldsymbol{T}} \cdot (\boldsymbol{K}_{\boldsymbol{W}} \cdot \boldsymbol{S}_{\boldsymbol{a}} \cdot \boldsymbol{K}_{\boldsymbol{W}}^{\boldsymbol{T}} + \boldsymbol{S}_{\boldsymbol{\varepsilon}})^{-\mathbf{1}} \cdot \boldsymbol{K}_{\boldsymbol{W}} = \\ &= (\boldsymbol{K}_{\boldsymbol{W}}^{\boldsymbol{T}} \cdot \boldsymbol{S}_{\boldsymbol{\varepsilon}}^{-\mathbf{1}} \cdot \boldsymbol{K}_{\boldsymbol{W}} + \boldsymbol{S}_{\boldsymbol{a}}^{-\mathbf{1}})^{-\mathbf{1}} \cdot \boldsymbol{K}_{\boldsymbol{W}}^{\boldsymbol{T}} \cdot \boldsymbol{S}_{\boldsymbol{\varepsilon}}^{-\mathbf{1}} \cdot \boldsymbol{K}_{\boldsymbol{W}},\end{aligned} \tag{2.25}$$

where is highlighted in green the gain matrix, describes the vertical correlation between the parameters at different heights for a given set of frequency channels and it will be used to measure the entropy improvement by channel.

2.3 Channel Selection Methods

In this chapter, four different channel selection methods used are explained. Three of them are based on the analysis of the calculated weighting functions: Legendre Polynomials, the amount of Information Content, and the number of Degrees of Freedom, while the Electrical Path Delay method analyses directly the calculated Electrical Path Delay from the three generated atmospheres. For the four presented methods, only the Information Content based has been used to present the final results of this project.

In chapters 3 and 5 an overview of the results obtained for each method and the reasons why only last method was selected as the optimum one will be presented.

2.3.1 Channel Selection based on Legendre Polynomials

This methods uses the Legendre polynomials to measure the contribution of the atmospheric water vapor to the brightness temperature for all frequency channels studied.

From the discrete model defined in Eqn. 2.9 using the Legendre polynomials' ($g_n(x)$) theorem, the atmospheric water vapor $\rho_v(z)$ and the water vapor weighting function matrix $K_W(f,\theta,z)^{\uparrow}$ can be presented as non-orthogonal polynomials as follows:

$$f(x) = \sum_n a_n \cdot g_n(x) \rightarrow \rho_v(z) = \sum_n a_n \cdot K^{\uparrow}_{W_n}(z), \tag{2.26}$$

where a_n is the weight or contribution of the water vapor weighting function K_W into the profile water vapor ρ_v.

Multiplying both sides of Eqn. 2.26 by K_{W_m}, where m is fixed and represents the number of the channel:

$$\int_0^h K^{\uparrow}_{W_m}(z) \cdot \rho_v(z) dz = \sum_n a_n \cdot \int_0^h K^{\uparrow}_{W_m}(z) \cdot K^{\uparrow}_{W_n}(z) dz. \tag{2.27}$$

Equation 2.6 can then be written as in Eqns. 2.28, and 2.29:

$$\int_0^h K^{\uparrow}_{W_m}(z)\rho_v = T_{B_m} = \sum_n a_n \cdot \int_0^{hmax} K^{\uparrow}_{W_m}(z) \cdot K_{W_n}(z) dz, \tag{2.28}$$

$$\begin{pmatrix} T_{B_1} \\ T_{B_2} \\ T_{B_3} \\ \vdots \\ T_{B_N} \end{pmatrix} = \begin{pmatrix} \int_0^h K^{\uparrow}_{W_1} \cdot K^{\uparrow}_{W_1} dx & \int_0^h K^{\uparrow}_{W_1} \cdot K^{\uparrow}_{W_2} dx & \int_0^h K^{\uparrow}_{W_1} \cdot K^{\uparrow}_{W_3} dx & \cdots & \int_0^h K^{\uparrow}_{W_1} \cdot K^{\uparrow}_{W_M} dx \\ \int_0^h K^{\uparrow}_{W_2} \cdot K^{\uparrow}_{W_1} dx & \int_0^h K^{\uparrow}_{W_2} \cdot K^{\uparrow}_{W_2} dx & \int_0^h K^{\uparrow}_{W_2} \cdot K^{\uparrow}_{W_3} dx & \cdots & \int_0^h K^{\uparrow}_{W_2} \cdot K^{\uparrow}_{W_M} dx \\ \int_0^h K^{\uparrow}_{W_3} \cdot K^{\uparrow}_{W_1} dx & \int_0^h K^{\uparrow}_{W_3} \cdot K^{\uparrow}_{W_2} dx & \int_0^h K^{\uparrow}_{W_3} \cdot K^{\uparrow}_{W_3} dx & \cdots & \int_0^h K^{\uparrow}_{W_3} \cdot K^{\uparrow}_{W_M} dx \\ \vdots & \vdots & \vdots & \ddots & \vdots \\ \int_0^h K^{\uparrow}_{W_N} \cdot K^{\uparrow}_{W_1} dx & \int_0^h K^{\uparrow}_{W_N} \cdot K^{\uparrow}_{W_2} dx & \int_0^h K^{\uparrow}_{W_N} \cdot K^{\uparrow}_{W_3} dx & \cdots & \int_0^h K^{\uparrow}_{W_N} \cdot K^{\uparrow}_{W_M} dx \end{pmatrix} \cdot \begin{pmatrix} a_1 \\ a_2 \\ a_3 \\ \vdots \\ a_N \end{pmatrix}. \tag{2.29}$$

Therefore the vector of coefficients a_n can be calculated from the measurement vector $\boldsymbol{y} = \boldsymbol{T_B}$ and the weighting function matrix $\boldsymbol{K_W}$ as follows:

$$\boldsymbol{a} = \boldsymbol{G^{-1}} \cdot \boldsymbol{TB}, \tag{2.30}$$

where $\boldsymbol{a}$ is the vector that contains all a_n coefficients, $\boldsymbol{G}$ is the weighting function covariance matrix, and $\boldsymbol{T_B}$ is the matrix that contains all calculated temperatures.

This vector indicates numerically which channels provide more information about the atmospheric water vapor profile ρ_v.

Finally, the error in the estimation for each frequency channel can be evaluated as:

$$\varepsilon = ||T_{B_n} - \sum_{n=1}^{N'<N} a_n \cdot \left(\int_0^h K^{\uparrow}_{W_m}(z) \cdot K^{\uparrow}_{W_n},(z)\,dz \right)||^2. \tag{2.31}$$

2.3.2 Channel Selection based on the amount of Information Content

This methodology is the one finally used in this project, and consist of the analysis of the sensibility to atmospheric water vapor content of the down-looking brightness temperatures measured from the space, and the evaluation of the optimum set of frequency channels that provide the largest amount of information on the water vapor content, i.e. the information provided by the selected channels is most uncorrelated. Once a channel is selected, the information provided is considered at the time to select further channels, avoiding redundant data.

Information Content

To compute the information content of the different channels the concept of entropy of the probability density functions is used as defined by Shannon in Information Theory [7]. The quantity of information of a given parameter that is provided by some observations (frequency channel) is computed as the change in the information entropy from a prior knowledge state of this parameter, and its knowledge after that observation. This is expressed in Eqns. 2.32 and 2.33, where the analyzed state is $\boldsymbol{x}$, the observations are $\boldsymbol{y}$, S indicates the entropy of the state with probability P, and H is the reduction in the entropy or information content.

$$H_n = S[P(\boldsymbol{x})] - S[P(\boldsymbol{x}|\hat{\boldsymbol{y}}], \tag{2.32}$$

$$H_m = S[P(\hat{\boldsymbol{y}}] - S[P(\hat{\boldsymbol{y}}|\boldsymbol{x})]. \tag{2.33}$$

In Eqn. 2.32 the entropy reduction is evaluated in the state space or atmospheric profile, i.e. the change in the entropy of the state vector when it is improved by the measurements, where the subscript n is the number of atmospheric layers. In Eqn. 2.33 the reduction entropy is evaluated in measurement space, i.e. the change in the entropy of the measurements when there is previous knowledge about the state space, where the subscript m is the number of observation channels (or frequencies). The result obtained for each equation is the same, and could be combined to measure the reduction entropy when other channels are previously selected.

Information on a Probability Density Function

Based on Shannon's definition of discrete information systems, where the probability density function is its measure of knowledge and, on Gibbs' definition of thermodynamic entropy, where the entropy of a thermodynamic system is the number of distinct internal states as pressure, temperature, water vapor... the discrete entropy of a radiometric system with probability P is expressed as:

$$S(P) = -k \cdot \sum_i p_i \cdot log_2 p_i, \tag{2.34}$$

where k is the Boltzmann constant and it is equal to 1 in information theory. For a continuous probability density function, where p_i corresponds to $P(x)dx$ the entropy is redefined as:

$$S(P) = -\int P(x) \cdot log_2[P(x)/M(x)] \cdot dx, \tag{2.35}$$

where dx is taken by a measurement function M that can also be interpreted as a prior probability density function.

Finally, as described in Eqns. 2.32, and 2.33, the information content of a system where P_1 describes its knowledge before the measurement and P_2 describes it afterwards, is the reduction in the entropy:

$$H = S(P_1) - S(P_2). \tag{2.36}$$

In this work the probability distribution of the observations is assumed to be Gaussian, so that, the Eqn. 2.35 is expressed as:

$$S = \frac{1}{(2\pi)^{1/2} \cdot \sigma} \cdot \int exp\left\{-\frac{(x-\hat{x})^2}{2 \cdot \sigma^2}\right\} \cdot \left(log_2[(2\pi)^{1/2} \cdot \sigma] + \frac{(x-\hat{x})}{2\sigma^2}\right). \tag{2.37}$$

On the other hand, Eqns. 2.12 and 2.11 can be seen to be related to the scalar Gaussian distribution by transforming to a basis which the covariance matrices $\boldsymbol{S_y}$ and $\boldsymbol{S_a}$ are diagonal, using the eigenvector decomposition $\boldsymbol{S} = \boldsymbol{L} \cdot \boldsymbol{\Delta} \cdot \boldsymbol{Ł}^{\boldsymbol{T}}$

$$\begin{aligned} P(y) &= \frac{1}{(2\pi)^{n/2}|\boldsymbol{L} \cdot \boldsymbol{\Delta} \cdot \boldsymbol{L^T}|} \cdot exp\left\{-\frac{1}{2} \cdot (\boldsymbol{y} - \hat{\boldsymbol{y}}) \cdot \boldsymbol{L} \cdot \boldsymbol{\Delta^{-1}} \cdot \boldsymbol{L^T} \cdot (\boldsymbol{y} - \hat{\boldsymbol{y}})\right\} = \\ &= \frac{1}{(2\pi)^{n/2} \cdot |\boldsymbol{\Delta}|} \cdot exp\left\{-\frac{1}{2} \cdot \boldsymbol{z^T} \cdot \boldsymbol{\Delta^{-1}} \cdot \boldsymbol{z}\right\}, \end{aligned} \tag{2.38}$$

where $\boldsymbol{z} = \boldsymbol{L^T} \cdot (\boldsymbol{y} - \hat{\boldsymbol{y}})$. Finally, the probability density function can be written as a product of the independent probability density functions' of each element of $\boldsymbol{z}$:

$$P(\boldsymbol{z}) = \prod_i \frac{1}{(2\pi \cdot \lambda_i)^{1/2}} \cdot exp\left\{-\frac{z_i^2}{2 \cdot \lambda_i}\right\}, \tag{2.39}$$

where the eigenvalue λ_i is the variance of z_i.

Thus, using Eqn. 2.39, for a vector with m total number of elements, the entropy of a multivariate Gaussian distribution is:

$$\begin{aligned} S[P(\boldsymbol{y})] &= \sum_{i=1}^{m} log_2(2\pi \cdot e \cdot \lambda_i)^{\frac{1}{2}} = \\ &= m \cdot log_2(2\pi \cdot e)^{\frac{1}{2}} + \frac{1}{2} \cdot log_2(\prod_i \lambda_i) = \\ &= m \cdot log_2(2\pi \cdot e)^{\frac{1}{2}} + \frac{1}{2} \cdot log_2|\boldsymbol{S_y}| \approx \frac{1}{2} \cdot log_2|\boldsymbol{S_y}|. \end{aligned} \tag{2.40}$$

Therefore the Eqn. 2.36 can be rewritten using Eqn. 2.40 as:

$$H = \frac{1}{2} \cdot log_2|\boldsymbol{S_1}| - \frac{1}{2} \cdot log_2|\boldsymbol{S_2}| = \frac{1}{2} \cdot log_2|\boldsymbol{S_1} \cdot \boldsymbol{S_2^{-1}}| = -\frac{1}{2} \cdot log_2|\boldsymbol{S_2} \cdot \boldsymbol{S_1^{-1}}|, \tag{2.41}$$

Channel Selection by an Iterative Method

The method used to select the optimum set of frequencies consists of the evaluation of the information content of each individual frequency channel, and considering the previously selected ones using Eqns. 2.32 and 2.33. Equation 2.33 evaluates the change of the measures' entropy caused by each selected channel which, at the same time, changes the vertical entropy as expressed in Eqn. 2.32.

Once the entropy for a discrete multivariate Gaussian distributions (Eqn. 2.41) is defined, the entropy reduction in the measurement and state spaces (Eqns. 2.32 and 2.33) can be analyzed. Starting on the state space from Eqn. 2.41, where the entropy reduction is measured in the state vector $\boldsymbol{x}$, with total number of elements (atmosphere layers) n, the entropy reduction (Eqn. 2.32) is expressed as:

$$H_n = S[P(\boldsymbol{x})] - S[P(\boldsymbol{x}|\hat{\boldsymbol{y}})] = \frac{1}{2} \cdot log_2|\boldsymbol{S_a}| - \frac{1}{2} log_2|\hat{\boldsymbol{S}}| = \frac{1}{2} \cdot log_2|\hat{\boldsymbol{S}}^{-1} \cdot \boldsymbol{S_a}|, \tag{2.42}$$

that can also be written as:

$$H_n = -\frac{1}{2} \cdot log_2 |\hat{\boldsymbol{S}} \cdot \boldsymbol{S_a^{-1}}|, \tag{2.43}$$

where, from the Averaging Kernel definition of Eqn. 2.25:

$$\boldsymbol{I} - \boldsymbol{AK} = (\boldsymbol{K_W^T} \cdot \boldsymbol{S_\varepsilon^{-1}} \cdot \boldsymbol{K_W} + \boldsymbol{S_a^{-1}})^{-1} \cdot \boldsymbol{S_a^{-1}} = \hat{\boldsymbol{S}} \cdot \boldsymbol{S_a^{-1}}. \tag{2.44}$$

Finally, Eqn. 2.42 can be presented as:

$$H_n = -\frac{1}{2} \cdot log_2 |\boldsymbol{I_n} - \boldsymbol{AK}|. \tag{2.45}$$

On the other hand, the entropy reduction in the measurement space in Eqn. 2.33 (temperatures observed in each channel m) can be expressed as Eqn. 2.46, and the change on the information content for the measurement vector $\boldsymbol{y}$ with m total number of observations (frequency channels) is computed as:

$$\begin{aligned} H_m &= S[P(\hat{\boldsymbol{y}})] - S[P(\hat{\boldsymbol{y}}|\boldsymbol{x})] = \frac{1}{2} \cdot log_2 |\boldsymbol{S_\varepsilon^{-1}} \cdot (\boldsymbol{K_W} \cdot \boldsymbol{S_a} \cdot (\boldsymbol{K_W^T} + \boldsymbol{S_\varepsilon})| = \\ &= \frac{1}{2} log_2 |\boldsymbol{S_\varepsilon^{-\frac{1}{2}}} \cdot \boldsymbol{K_W} \cdot \boldsymbol{S_a} \cdot \boldsymbol{K_W^T} \cdot \boldsymbol{S_\varepsilon^{-\frac{1}{2}}} + \boldsymbol{I_m}|, \end{aligned} \tag{2.46}$$

where the covariance of $\boldsymbol{y}$ before the measurement is

$$\begin{aligned} \boldsymbol{S_{y_a}} &= E\{(\boldsymbol{y} - \boldsymbol{y_a}) \cdot (\boldsymbol{y} - \boldsymbol{y_a})^{\boldsymbol{T}}\} = \\ &= E\{\boldsymbol{K_W} \cdot (\boldsymbol{x} - \boldsymbol{x_a}) \cdot (\boldsymbol{x} - \boldsymbol{x_a})^{\boldsymbol{T}} \cdot \boldsymbol{K_W^T} + \boldsymbol{\varepsilon} \cdot \boldsymbol{\varepsilon}^{\boldsymbol{T}}\} = \boldsymbol{K_W} \cdot \boldsymbol{S_a} \cdot \boldsymbol{K_W^T} + \boldsymbol{S_\varepsilon}. \end{aligned} \tag{2.47}$$

The iterative method consists of measuring the entropy of a set of frequency channels, and selecting the one that provides more information. This process is repeated iteratively, where the information provided by the remaining channels is evaluated based on the information provided by the previously selected ones. It means that Eqn. 2.46 has to be updated iteratively.

Equation 2.46 compares the entropy of the measurements ($S[P(\hat{\boldsymbol{y}})]$) with the entropy improvement by the knowledge of the state space ($S[P(\hat{\boldsymbol{y}}|\boldsymbol{x})]$). Therefore the entropy of the state space will change according to the selected channels, and Eqn. 2.46 can be rewritten as:

$$H_m = \frac{1}{2} \cdot log_2 |\boldsymbol{K_W'} \cdot \boldsymbol{A} \cdot \boldsymbol{K_W'^T} + \boldsymbol{I_m}|, \tag{2.48}$$

where $\boldsymbol{K'_W} = \boldsymbol{S_\varepsilon^{-\frac{1}{2}}} \cdot \boldsymbol{K_W}$ and the covariance matrix of the state vector $\boldsymbol{S_a}$ in Eqn. 2.46 are replaced by the matrix $\boldsymbol{A}$, that considers the improvement on the state vector due to the channels already selected, and it is given by:

$$\boldsymbol{A} = [\boldsymbol{I_n} - \boldsymbol{S_a} \cdot \boldsymbol{K_W^T} \cdot (\boldsymbol{K_W} \cdot \boldsymbol{S_a} \cdot \boldsymbol{K_W^T} + \boldsymbol{S_\varepsilon})^{-1} \cdot \boldsymbol{K_W}] \cdot \boldsymbol{S_a} = [\boldsymbol{I_n} - \boldsymbol{AK}] \cdot \boldsymbol{S_a}, \tag{2.49}$$

which gives the covariance matrix of the state vector $\boldsymbol{S_a}$, updated with the frequency channels, as expressed in Eqn. 2.45:

$$\begin{aligned} \frac{1}{2} \cdot log_2[\boldsymbol{A}] = \frac{1}{2} \cdot log_2|(\boldsymbol{I_n} - \boldsymbol{AK}) \cdot \boldsymbol{S_a}| = \frac{1}{2} \left[log_2|\boldsymbol{I_n} - \boldsymbol{AK}| + log_2|\boldsymbol{S_a}| \right] = \\ = \frac{1}{2} \cdot log_2|\boldsymbol{S_a}| - H_n. \end{aligned} \tag{2.50}$$

Thus, when there is no channel selected ($\boldsymbol{I_n} - \boldsymbol{AK} = I_n$) from Eqn. 2.49 $\boldsymbol{A} = \boldsymbol{S_a}$ is obtained. Applying this result in Eqn. 2.48 gives: $H_m = \frac{1}{2} \cdot \boldsymbol{log_2}|\boldsymbol{K'_W} \cdot \boldsymbol{S_a} \cdot \boldsymbol{K'^T_W} + \boldsymbol{I_m}|$, that corresponds with Eqn. 2.46. Also, assuming that $\boldsymbol{A} = \boldsymbol{S_a}$ Eqn. 2.45 gives 0. The first assumption indicates that when any channel is selected, the entropy reduction in the measurement space H_m, remains constant and depends only on the state vector ($\boldsymbol{S_a}$, n levels). The second assumption indicates that as there is no channel selected, the entropy reduction in the state vector (H_n) is null ($m = 0$ channels improving the entropy).

Finally, the evaluation of the information content for one single frequency i using Eqn. 2.48 is:

$$\delta ER_i = \frac{1}{2} \cdot log_2[1 + \boldsymbol{k'_{W_i}} \cdot \boldsymbol{A_{i-1}} \cdot \boldsymbol{k'^T_W}], \tag{2.51}$$

where

$$\boldsymbol{A_i} = \boldsymbol{A_{i-1}} - \frac{(\boldsymbol{A_{i-1}} \cdot \boldsymbol{k'^T_{W_i}}) \cdot (\boldsymbol{A_{i-1}} \cdot \boldsymbol{k'^T_{W_i}})^T}{\boldsymbol{1} + (\boldsymbol{A_{i-1}} \cdot \boldsymbol{k'^T_{W_i}}) \cdot \boldsymbol{k'^T_{W_i}}}, \tag{2.52}$$

and as mentioned above $\boldsymbol{A_0} \triangleq \boldsymbol{S_a}$

2.3.3 Channel Selection based on the number of Degrees of Freedom

The method of the degrees of freedom consists of determining the number of independent pieces of information in a set of measurements [7]. That is, from a set of frequency channels,

determine which ones provide most uncorrelated information about the state of the atmosphere. This method uses the iterative method presented in the Information Content method to update the covariance matrix of the state vector $\boldsymbol{S_a}$, giving similar results. The difference of both methods (the one based on the amount of Information and the one based on the number of Degrees of Freedom) is the measure used to evaluate the channel contribution in each one. For the amount of Information Content methods, the change on the atmosphere's stateinformation get in the beginning (any channel selected) is evaluated. However, in the number of Degrees of Freedom based method, the number of independent measurements over the noise or error are computed.

Let's consider the model presented in Eqn. 2.9, for one observation where x has prior variance σ_a^2, and $\boldsymbol{\varepsilon}$ has σ_ε^2. In the number of degrees of freedom χ can be estimated as:

$$\chi = \frac{\sigma_\epsilon^2 \cdot \chi_a + \sigma_a^2 \cdot \chi_\epsilon}{\sigma_\epsilon^2 + \sigma_a^2}, \tag{2.53}$$

where χ_a and χ_ϵ are the number of degrees of freedom for the state vector and the noise or error vector respectively.

Thus, in case $\sigma_a^2 << \sigma_\varepsilon^2$ y is providing information about the state value x, otherwise, y is providing information about the measurement error ε.

Applying the same approach for a case of m number of measurements and n number of states in the atmosphere where the measurements have a linear Gaussian distribution, Eqn. 2.53 can be presented as:

$$\chi^2 = (\boldsymbol{x} - \boldsymbol{x_a})^T \cdot \boldsymbol{S_a^{-1}} \cdot (\boldsymbol{x} - \boldsymbol{x_a}) + \boldsymbol{\epsilon}^T \cdot \boldsymbol{S_\epsilon^{-1}} \cdot \boldsymbol{\epsilon}. \tag{2.54}$$

To avoid off-diagonal elements in the covariance matrices, caused by correlations between the variability of different elements of the vectors, a change of base is needed for the measurements vector as shown in the following equation:

$$\hat{\boldsymbol{y}} = \boldsymbol{S_\varepsilon^{-\frac{1}{2}}} \cdot \boldsymbol{K_W} \cdot \boldsymbol{S_a^{\frac{1}{2}}} \cdot \hat{\boldsymbol{x}} + \boldsymbol{S_\varepsilon^{-\frac{1}{2}}} \cdot \boldsymbol{\varepsilon} = \hat{\boldsymbol{K}}_{\boldsymbol{W}} \cdot \hat{\boldsymbol{x}} + \hat{\boldsymbol{\varepsilon}}. \tag{2.55}$$

As explained above, the degrees of freedom measure both the amount of independent information of noise and the state of the atmosphere. Thus, Eqn. 2.54 can be clearly divided in two equations, Eqn. 2.56 and Eqn. 2.57, that refer to degrees of freedom of the state of the atmosphere $\boldsymbol{x}$ and degrees of freedom of the measurement error $\boldsymbol{\varepsilon}$ respectively:

$$d_s = E\{(\hat{\boldsymbol{x}} - \boldsymbol{x_a})^{\boldsymbol{T}} \cdot \boldsymbol{S_a^{-1}} \cdot (\hat{\boldsymbol{x}} - \boldsymbol{x_a})\}, \tag{2.56}$$

$$d_n = E\{\hat{\boldsymbol{\varepsilon}}^{\boldsymbol{T}} \cdot \boldsymbol{S_\varepsilon^{-1}} \cdot \hat{\boldsymbol{\varepsilon}}\}. \tag{2.57}$$

Covariance matrix used in Eqns. 2.56 and 2.57 ($\boldsymbol{S_a}$) is assumed to be diagonal, then matrix trace properties can be used to define an explicit expression for both equations:

$$\begin{aligned} d_s &= E\{(\hat{\boldsymbol{x}} - \boldsymbol{x_a})^{\boldsymbol{T}} \cdot \boldsymbol{S_a^{-1}} \cdot (\hat{\boldsymbol{x}} - \boldsymbol{x_a})\} = \\ &= E\{tr[(\hat{\boldsymbol{x}} - \boldsymbol{x_a}) \cdot (\hat{\boldsymbol{x}} - \boldsymbol{x_a})^{\boldsymbol{T}} \cdot \boldsymbol{S_a^{-1}}]\} = tr(\boldsymbol{S_{\hat{x}}} \cdot \boldsymbol{S_a^{-1}}), \end{aligned} \tag{2.58}$$

where from Eqns. 2.55 and 2.23

$$\begin{aligned} \boldsymbol{S_{\hat{x}}} &= \boldsymbol{E}\{(\hat{\boldsymbol{x}} - \boldsymbol{x_a}) \cdot (\hat{\boldsymbol{x}} - \boldsymbol{x_a})^{\boldsymbol{T}}\} = \\ &= \boldsymbol{G} \cdot (\boldsymbol{K_W} \cdot \boldsymbol{S_a} \cdot \boldsymbol{K_W^T} + \boldsymbol{S_\varepsilon} \cdot \boldsymbol{G^T}) = \\ &= \boldsymbol{S_a} \cdot \boldsymbol{K_W^T} \cdot (\boldsymbol{K_W} \cdot \boldsymbol{S_a} \cdot \boldsymbol{K_W^T} + \boldsymbol{S_\varepsilon})^{\boldsymbol{-1}} \cdot \boldsymbol{K_W} \cdot \boldsymbol{S_a}. \end{aligned} \tag{2.59}$$

Then, combining Eqns. 2.59 and 2.23

$$\begin{aligned} d_s &= tr(\boldsymbol{S_a} \cdot \boldsymbol{K_W^T} \cdot [\boldsymbol{K_W} \cdot \boldsymbol{S_a} \cdot \boldsymbol{K_W^T} + \boldsymbol{S_\varepsilon}]^{\boldsymbol{-1}} \cdot \boldsymbol{K_W}) = \\ &= tr(\boldsymbol{K_W} \cdot \boldsymbol{S_a} \cdot \boldsymbol{K_W^T} \cdot [\boldsymbol{K_W} \cdot \boldsymbol{S_a} \cdot \boldsymbol{K_W^T} + \boldsymbol{S_\varepsilon}]^{\boldsymbol{-1}}) = \\ &= tr([\boldsymbol{K_W^T} \cdot \boldsymbol{S_\varepsilon^{-1}} \cdot \boldsymbol{K_W} + \boldsymbol{S_a^{-1}}]^{\boldsymbol{-1}} \cdot \boldsymbol{K_W^T} \cdot \boldsymbol{S_\varepsilon^{-1}} \cdot \boldsymbol{K_W}). \end{aligned} \tag{2.60}$$

Likewise, for the degrees of freedom of the error measurement $\boldsymbol{\varepsilon}$:

$$\begin{aligned} d_n &= tr(\boldsymbol{S_a} \cdot \boldsymbol{K_W^T} \cdot [\boldsymbol{K_W} \cdot \boldsymbol{S_a} \cdot \boldsymbol{K_W^T} + \boldsymbol{S_\varepsilon}]^{\boldsymbol{-1}} \cdot \boldsymbol{K_W}) = \\ &= tr([\boldsymbol{K_W^T} \cdot \boldsymbol{S_\varepsilon^{-1}} \cdot \boldsymbol{K_W} + \boldsymbol{S_a^{-1}}]^{\boldsymbol{-1}} \cdot \boldsymbol{S_a^{-1}}). \end{aligned} \tag{2.61}$$

Finally, considering that the measurement vector has the contributions of both the state of the atmosphere and the measurement error, the total number of degrees of freedom evaluated for all the set of channels m should be equal to the total number of frequency channels m, i.e. $d_s + d_s = tr(\boldsymbol{I_m})$.

Equation 2.59 corresponds to the covariance matrix of the state vector, that from Eqn. 2.59 can be rewritten as:

$$\boldsymbol{S_{\hat{x}}} = [\boldsymbol{S_a} - \boldsymbol{A}], \tag{2.62}$$

thus, Eqn. 2.58 becomes:

$$d_s = tr[(\boldsymbol{S_a} - \boldsymbol{A}) \cdot \boldsymbol{S_a^{-1}}] = \boldsymbol{tr}[\boldsymbol{I_n} - \boldsymbol{A} \cdot \boldsymbol{S_a^{-1}}]. \tag{2.63}$$

Considering as in the amount of Information Content method that the $\boldsymbol{A}$ matrix is updated at each i iteration accordingly to the remaining or selected frequency channels [9], and $\boldsymbol{A_0} \triangleq \boldsymbol{S_a}$, Eqn. 2.63 can now be expressed as:

$$d_s = \boldsymbol{tr}[\boldsymbol{A_{i-1}} - \boldsymbol{A_i} \cdot \boldsymbol{S_a^{-1}}], \tag{2.64}$$

where for the first iteration $i = 1$, the general equation shown in 2.63 is obtained .

2.3.4 Channel Selection based on Electrical Path Delay

Unlike the other methods, this method focuses in the wet Electrical Path Delay calculated for the three generated atmospheres (temperate, tropical, and polar climates) to measure the contribution of the atmospheric water vapor into the measured brightness temperature.

The wet electrical path delay is the case of study of this project. It is calculated as the integral of refractivity due to the gases from the surface until the observation point, in this case, the altimetry radiometer:

$$\Delta L = \int_0^\infty N \cdot 10^6, \tag{2.65}$$

that at the same time is calculated as a function of the water vapor and oxygen gas atmospheric distribution:

$$N = k_1 \cdot \frac{R}{m_d} \cdot \rho_d(z) + \frac{R}{m_W} \cdot \rho_v(z) \cdot [k_2 + \frac{k_3}{T(z)}] = N_d + N_W, \tag{2.66}$$

where in Eqn. 2.66 he refractivity caused by atmospheric gases is highlighted in red and the refractivity caused by water vapor in orange.

Thus the electrical path delay caused by water vapor can be defined as:

$$\Delta L_W = \int_0^\infty N_W. \tag{2.67}$$

The delay on Eqn. 2.67 can be expressed as a weighted sum of the brightness temperatures as:

$$\Delta L_W = c_0 + \sum_{i=1}^{N} c_i \cdot \boldsymbol{T_{B_i}}, \tag{2.68}$$

where c_i coefficients denote the contribution of the water vapor content present in observations to the refractivity N_W, and the subindex i indicates the frequency channel number.

Algebraically Eqn. 2.68 is presented in Eqn. 2.69

$$\begin{pmatrix} \Delta L_{W_1} \\ \Delta L_{W_2} \\ \Delta L_{W_3} \\ \vdots \\ \Delta L_{W_M} \end{pmatrix} = \begin{pmatrix} 1 & T_{B_1}(f_1) & T_{B_1}(f_2) & T_{B_1}(f_3) & \cdots & T_{B_1}(f_N) \\ 1 & T_{B_2}(f_1) & T_{B_2}(f_2) & T_{B_2}(f_3) & \cdots & T_{B_2}(f_N) \\ 1 & T_{B_3}(f_1) & T_{B_3}(f_2) & T_{B_3}(f_3) & \cdots & T_{B_3}(f_N) \\ \vdots & \vdots & \vdots & \ddots & \vdots & \\ 1 & T_{B_M}(f_1) & T_{B_M}(f_2) & T_{B_M}(f_3) & \cdots & T_{B_N}(f_N) \end{pmatrix} \cdot \begin{pmatrix} c_0 \\ c_1 \\ c_2 \\ \vdots \\ c_N \end{pmatrix}. \tag{2.69}$$

In Eqn. 2.69 are evaluated MxN total number of observations, where N denotes the number of frequency channels and M the number of different evaluated atmospheric conditions for the three different climates (temperate, tropical, and polar). The M possible atmospheric conditions have been generated combining the input parameters: temperature $T(z)$, pressure $P(z)$, and water vapor $\rho_v(z)$.

Finally, the weight coefficients' vector c is calculated as:

$$\boldsymbol{c} = \boldsymbol{T_B^{-1}} \cdot \boldsymbol{\Delta L_W}, \tag{2.70}$$

that would be more accurate as much different atmospheres are generated.

For the four presented methods, just three are based on the weighting function matrix (Legendre Polynomials, amount of Information Content, and number of Degrees of Freedom method). From these three methods, in the Legendre Polynomials method, all the available set of frequency channels are evaluated in one iteration. It causes that the quality of the information retrieved does not depend on the sequence of the channel selection. That means that the information provided by a set of channels (frequencies) when a lower frequency channel has been previously selected will not vary in case that a higher frequency channel is previously selected instead. Otherwise, in the amount of Information Content and number of Degrees of Freedom methods, each iteration (selection order) is independently evaluated.

On the other hand, in the Electrical Path Delay method different atmospheric situations are evaluated. So the more accurate the samples are, the results will be better. Using virtual information (generated from a software) as mentioned is this work, limits the accuracy of this method.

CHAPTER 3

CHANNEL SELECTION METHODS: SIMULATIONS

In this chapter, the results for the four different channel selection methods explained above are presented. The four methods are evaluated and compared using upwelling brightness temperature (T_{UP}) measurements, and the following presented figures will help to understand the results obtained. Figure 3.1 shows the atmospheric gas absorption caused by the Oxygen and the water vapor, and the figures 3.2, and 3.3 show the impact of the water vapor in the bands' transmissivity for the three different climates (temperate, tropical, and polar).

Figure 3.1 shows the attenuation (in dB) caused by the atmospheric gases (Oxygen in red and water vapor in blue). For the water vapor, there are two peaks around 22.235 GHz and 183.300 GHz, that correspond to the water vapor resonance frequencies. The analysis of this report will be focused around these two frequencies. In this figure, the Oxygen absorption around 60 GHz and 120 GHz frequencies is clearly appreciable. Even though the aim of this project is to analyze the impact of water vapor in the radiometric measures, Oxygen absorption bands should also be taken into consideration. As it will be explained during this chapter, in the results obtained, numbers related with the Oxygen absorption will be presented together with the water vapor absorption ones, so it is necessary to identify which frequencies should not be considered when drawing conclusions.

Figures 3.2 and 3.3 have been computed from the atmospherics generated for this project. Figure 3.2 presents the zenith transmissivity from the Earth surface to the mesosphere for fre-

quencies between 5 GHz and 200 GHz. The two peaks of attenuation for atmospheric water vapor mentioned in the Fig. 3.1, have a clear impact in the atmospheric transmissivity. Around the lower resonance frequencies (22.235 GHz), the impact is smaller (Fig. 3.3). However for higher frequencies (183.300 GHz) the transmittance it is clearly reduced.

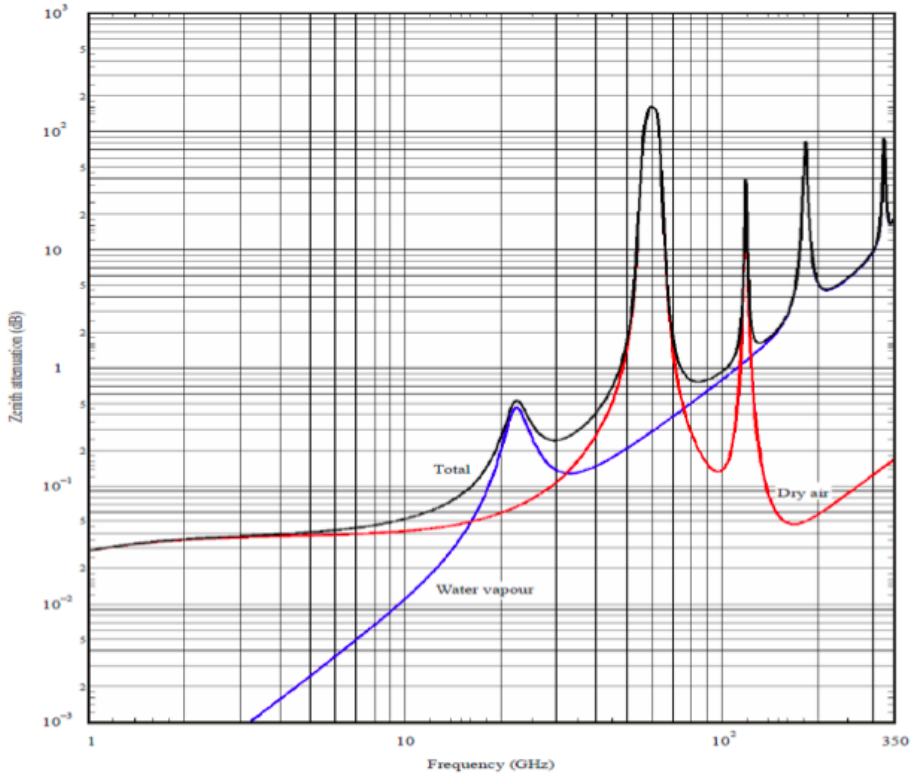

Figure 3.1: Atmospheric gaseous attenuation

In these figures can also be appreciated the importance of the climate when the atmospheric water vapor content is analyzed. It is clear the difference between the tropical and polar climates, where for the second case, in the lower frequencies, the presence of water vapor is practically negligible. While for the tropical climates, both frequencies seem to be suitable to retrieve water vapor information.

On the other hand, high resonance frequencies are more reactive with water vapor, meaning that they are suitable to detect its presence in the atmosphere. However this fact also means that high frequencies are the most attenuated ones, i.e. the most difficult to retrieve from the mesosphere. The importance of analyze higher and lower resonance frequencies lies in their

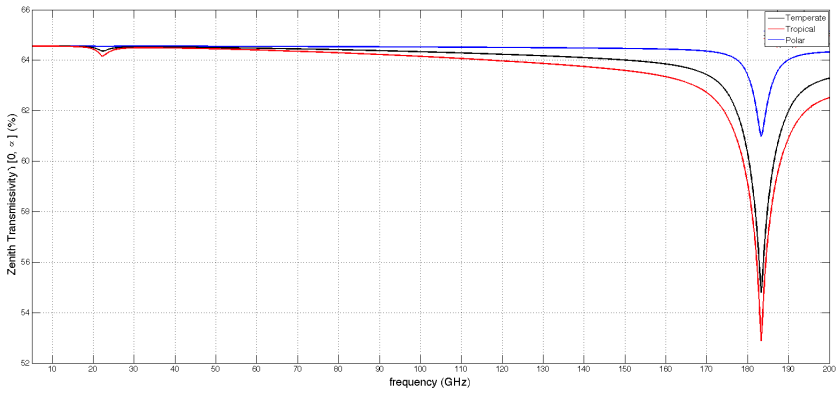

Figure 3.2: Transmissivity caused by the atmospheric water vapor

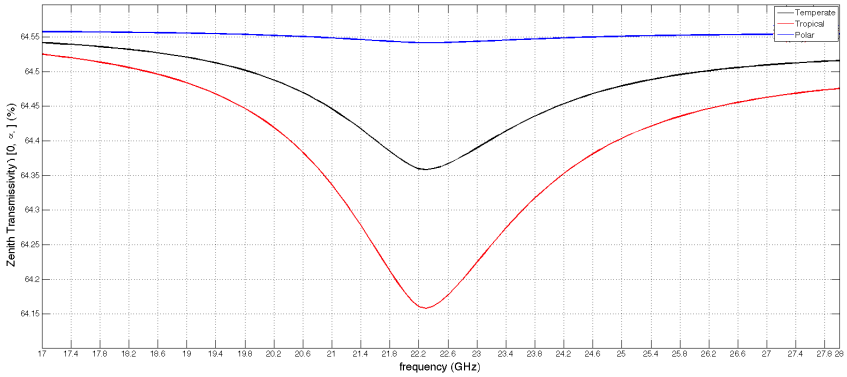

Figure 3.3: Transmissivity caused by the atmospheric water vapor for lower water vapor absorption bands

attenuation. Thus, in climates where there is a low content of water vapor in the atmosphere, like in the polar ones, higher resonance frequencies will be needed to its measure, while in tropical climates where there is a high concentration of water vapor in the atmosphere, with lower frequencies it will be enough.

3.1 Channel Selection based on Legendre Polynomials

By using the Legendre's Polynomials and based on the generated water vapor weighting functions, this method measures the presence of water vapor on each frequency channel's weighting function.

Graphical results focused on water vapor sounding frequencies (low and high bands) are presented in the Figs. 3.4, and 3.5 for the three climates (temperate, tropical, and polar). The corresponding numerical results are shown in the table 3.1.

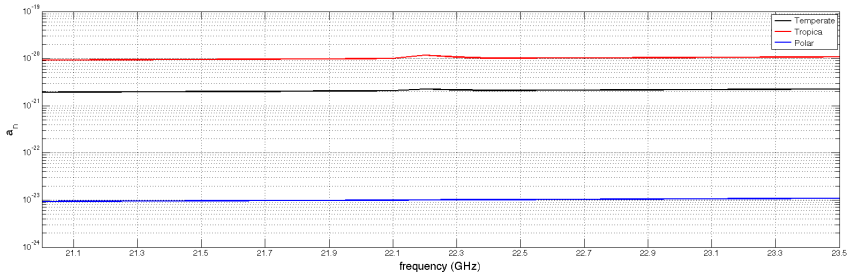

Figure 3.4: Legendre Polynomials for low frequency channels and the three climates (logarithmic scale)

Finally, in the Fig. 3.5 are presented the results for the high absorption water vapor frequencies.

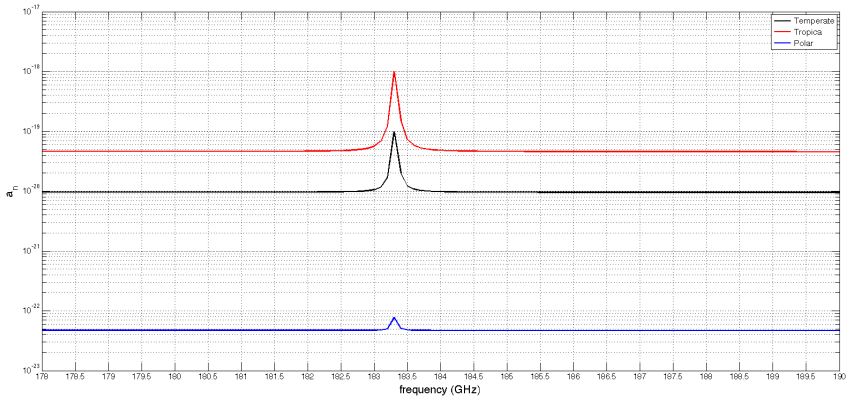

Figure 3.5: Legendre Polynomials for high frequency channels and the three climates (logarithmic scale)

In the figures it can be observed a peak around the resonant frequency channels (~ 22.235 GHz and ~ 183.300 GHz), fact that indicates that these frequency channels provide the most information about the atmospheric water vapor. Based on the gas attenuation profile of the atmosphere (Fig 3.1), these results are the expected ones, as they correspond to the resonance frequencies. However, transmissivity of the atmosphere (Figs. 3.2, 3.3, and **??**) should be also took into account. As is explained in this chapter, these frequency channels are indeed the

most reactive with the water vapor content but also the most attenuated along the atmosphere (~ 70 km), meaning that they can not be the optimum ones to retrieve information from a space borne radiometer.

Table 3.1: Legendre Polynomials for low and high frequency channels and the three climates

Temperate climate		**Tropical climate**		**Polar climate**	
f[GHz]	$a_n(10^{-21})$	**f[GHz]**	$a_n(10^{-20})$	**f[GHz]**	$a_n(10^{-23})$
22.2	2.246	22.2	1.187	22.0	0.990
22.3	2.162	22.3	1.084	22.1	0.9976
22.5	2.125	22.4	1.029	22.2	1.007
22.4	2.12	22.5	1.027	22.3	1.011
22.1	2.085	22.1	1.016	22.4	1.016
22.0	2.06	22.0	0.996	22.5	1.022
183.3	995.1	183.3	100.3	183.3	7.705
183.4	200.2	183.4	153.3	183.4	5.082
183.2	168.8	183.2	120.9	183.2	4.968
183.5	122.5	183.5	73.13	183.5	4.796
183.1	117.7	183.1	68.26	183.1	4.781
183.6	107.6	183.6	57.91	183.6	4.741
183.0	106.2	183.0	56.4	183.0	4.739

Another observable fact in the figures 3.4, and 3.5, is the high presence of water vapor when the frequency is increased. These incorrect values correspond to the attenuation of the nearest Oxygen absorption band (~ 60 GHz), meaning that with this method other it is not possible to differentiate between the different attenuation sources: water vapor and Oxygen.

3.2 Channel Selection based on the amount of Information Content

In the Information Content method, an iteration per channel to analyze is done. For each iteration, the channel that provides the most information about the atmosphere, and also the most uncorrelated information with the one already available, is selected. This information is evaluated at each layer of the atmosphere (60 layers along ~ 70 km), meaning that unlike the Electrical Path Delay based method, high attenuated frequencies that can not reach the space radiometer are properly evaluated.

In this section, it will be seen contrary to the Legendre Polynomials based method, that the tails of the resonance frequencies are considered the optimum ones to retrieve water vapor information. In case of the polar climate, the optimum frequencies are closer to the resonance

frequencies, as the water vapor content is lower than in the other two climates and the transmissivity higher (Figs. 3.2, 3.3, and **??**).

Figures 3.6 and 3.7 present the results for the low and high absorption frequency bands respectively, based on the upwelling brightness temperature (T_{UP}). In both figures, the first graph shows the optimum frequency channels where there is not any channel previously selected, while the second graph presents further iterations, considering the previously selected frequency channels. Numerical results are shown in the table 3.2.

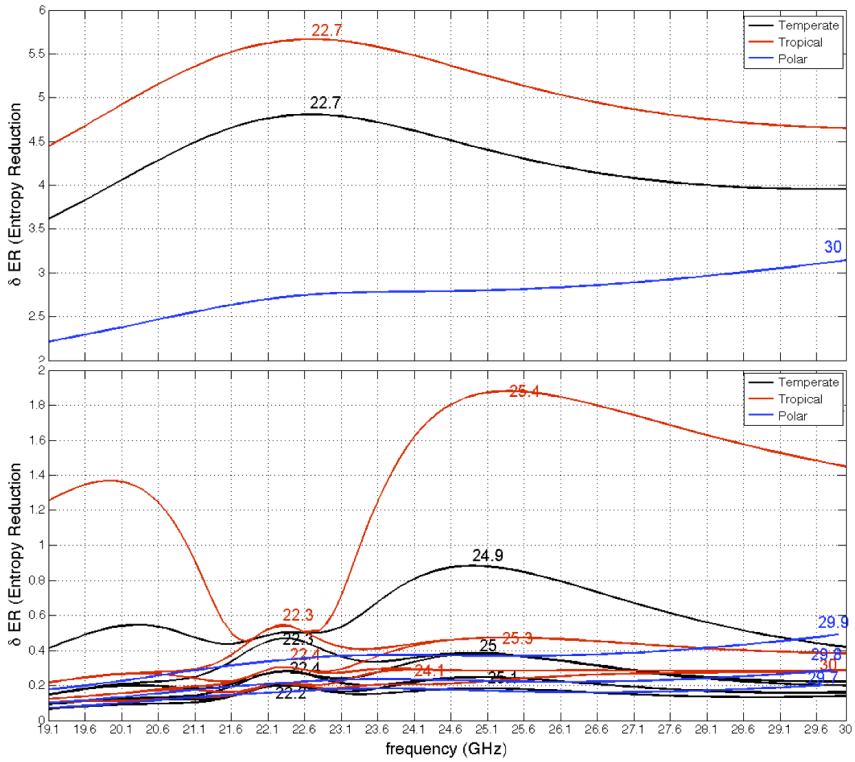

Figure 3.6: Entropy Reduction for lower frequencies and the three climates. Based on upwelling brightness temperature (T_{UP})

As occurs also in the number of Degrees of Freedom based method, in the first iterations (Figs. 3.6 and 3.7 first graph) it can be clearly observable that the first selected channel does not correspond with the sounding frequency channels (~ 23.235 GHz and 183.300 GHz). The resonant frequencies are the most reactive with the water vapor content, but also the most attenuated, i.e. they have lower transmittance from the surface, where there is a high water vapor content concentration, to the space. This attenuation or low transmittance in resonant

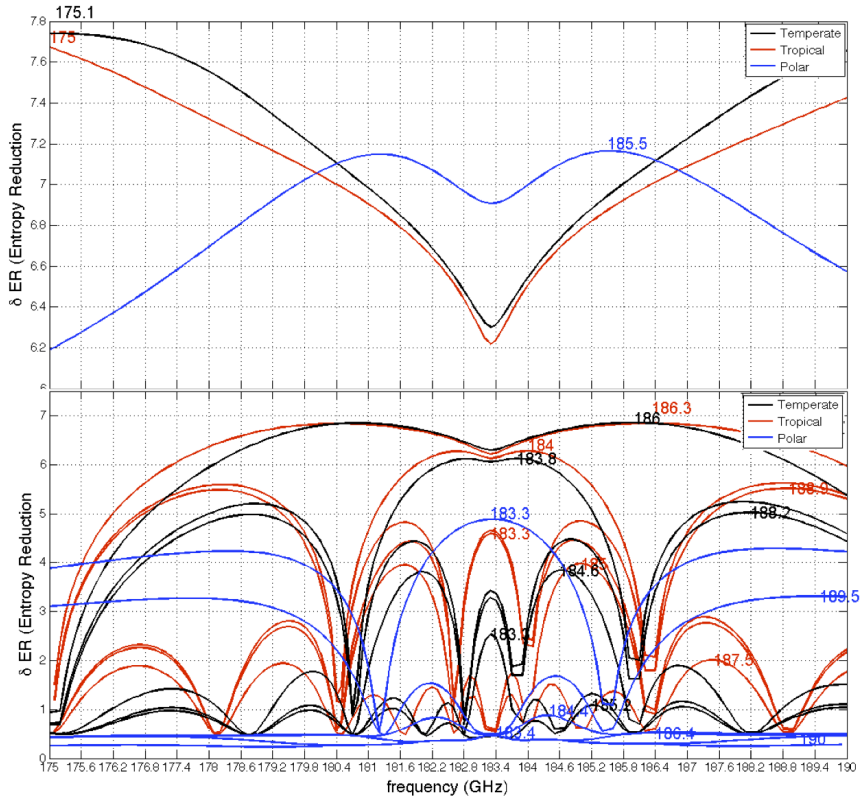

Figure 3.7: Entropy Reduction for higher frequencies and the three climates. Based on upwelling brightness temperature (T_{UP})

frequencies, causes that the information coming from the surface (T_{SC}) does not reach the space radiometer, making frequencies located in the tails the most optimal for this analysis.

After further iterations, (Figs. 3.6 and 3.7 second graph) sounding frequency channels (~ 23.235 GHz and 183.300 GHz) are selected. In the table 3.2 it can be seen that there is a big difference of information provided by these channels and the first selected ones (around 3 bits of information over a maximum of ~ 8 bits), contrary as the results obtained in the Legendre Polynomials analysis.

Table 3.2: Entropy reduction for low and high frequency channels and the three climates. Based on upwelling brightness temperature (T_{UP})

Temperate climate		**Tropical climate**		**Polar climate**	
f[GHz]	**ER[bits]**	**f[GHz]**	**ER[bits]**	**f[GHz]**	**ER[bits]**
22.7	4.807	22.7	5.666	30.0	3.141
24.9	0.883	25.4	1.881	29.9	0.490
22.3	0.469	22.3	0.540	29.8	0.286
25.0	0.380	25.3	0.473	29.7	0.202
22.4	0.279	22.4	0.303	29.6	0.156
25.1	0.246	24.1	0.289	23.6	0.135
22.2	0.199	30.0	0.284	23.7	0.114
175.1	7.740	175	7.673	185.5	7.164
186.0	6.586	185.3	6.843	183.3	4.879
183.8	6.120	184.0	6.275	189.5	3.312
188.2	5.021	188.9	5.515	184.4	0.878
184.6	3.848	183.3	4.594	186.4	0.522
183.3	2.539	185.0	3.980	190.0	0.467
185.2	1.091	187.5	2.010	183.4	0.461

3.3 Channel Selection based on the number of Degrees of Freedom

The number of Degrees of Freedom based method gives similar results as the Information Content based one. In this method, the degrees of freedom of the signal are used as a measure unit of uncorrelated information where, as explained in the previous chapter, the maximum number of degrees of freedom corresponds to the number of channels analyzed. In this case, as each channel is evaluated independently, the maximum is one.

In the Figs. 3.8, 3.9 (first iteration), and 3.10 (further iterations) the results for low and high frequency channels are presented, around the resonance frequencies 22.235 and 183.300 GHz, for the three climates (temperate, tropical, and polar) and based on the retrieved upwelling brightness temperature (T_{UP}). In the mentioned figures, like in the Information Content based method, it can be appreciated that for the three climates, the resonant frequencies (~ 22.235 GHz and ~ 183.300 GHz) are avoided to retrieve water vapor information, and frequencies in its tails are selected.

In these figures it is also shown that in the latest iterations, the sounding frequencies become the optimum ones when the frequencies from tails are already selected. Numerical results are shown in the table 3.3, where this behavior is evident in the fifth iteration of the tem-

perate climate for lower frequency channels, and in the last iteration for higher frequency channels in the same climate, in the last iteration for tropical climate and low and high frequency channels and, second iteration for polar climate and high frequency channels.

In all cases, due to the low water vapor content in the polar climate atmospheres, the frequencies selected provide much less information than in the other two climates and practically any information in the lower bands, that are less affected by the water vapor content.

Another effect to highlight for the lower frequency bands (Fig. 3.8), is the optimum frequency channels obtained near 30 GHz, that in case of polar climates, in the first graph it can be appreciated that exist a trend to these frequencies. This fact is again caused by the Oxygen absorption, that has a peak around 60 GHz.

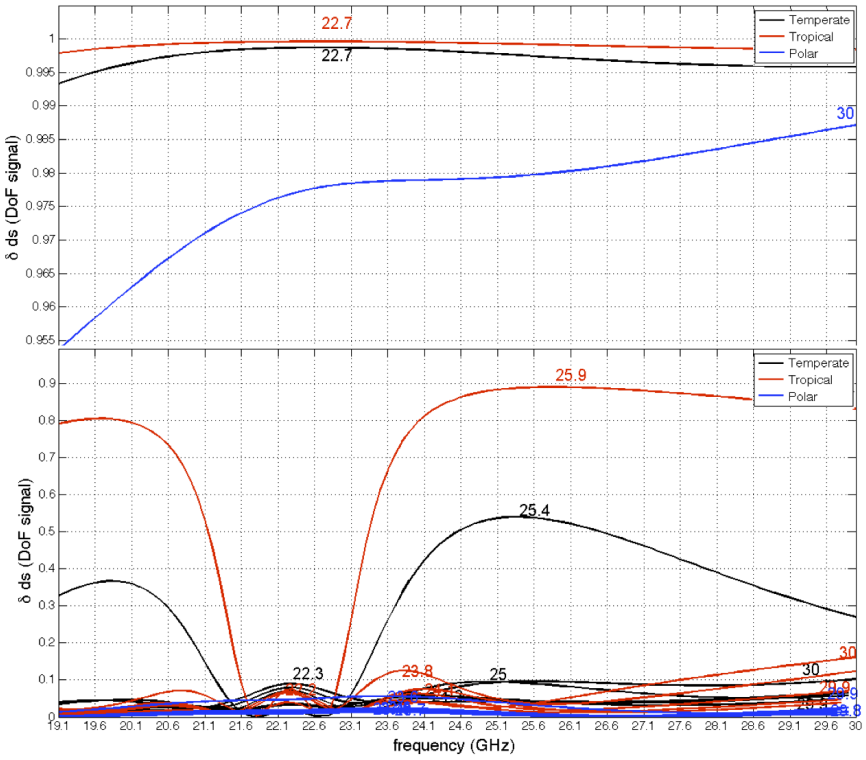

Figure 3.8: Degrees of freedom for low frequency channels and the three climates

The main difference between the Degrees of Freedom and the Information Content methods can be found in the figure 3.10, where it is difficult to graphically differentiate between the first three optimum frequencies for high absorption bands. As mentioned in the previously, the maximum number of degrees of freedom corresponds to the total number of observation

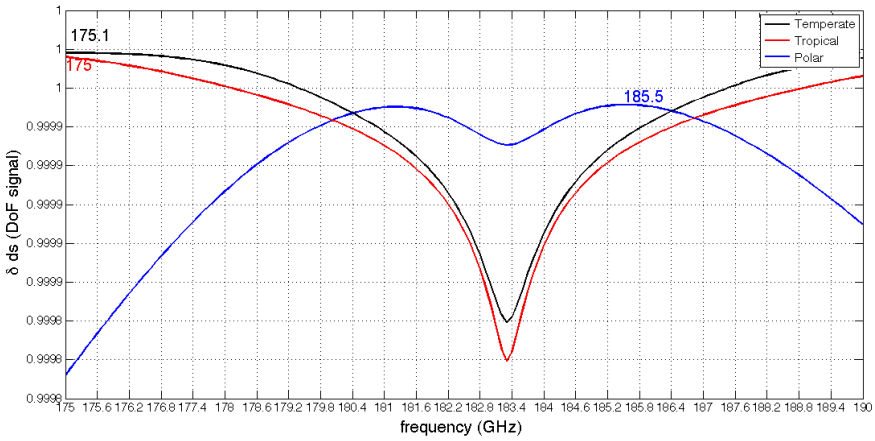

Figure 3.9: Degrees of freedom for high frequency channels and the three climates (1st iteration)

Table 3.3: Degrees of freedom for low and high frequency channels and the three climates

Temperate climate		**Tropical climate**		**Polar climate**	
f[GHz]	**DoF (signal)**	**f[GHz]**	**DoF (signal)**	**f[GHz]**	**DoF (signal)**
22.7	0.999	22.7	1.000	30.0	0.987
25.4	0.540	25.9	0.892	23.6	0.056
30.0	0.102	23.8	0.125	23.5	0.024
25.0	0.096	30.0	0.162	29.9	0.026
22.3	0.090	29.9	0.071	23.4	0.023
29.9	0.070	24.1	0.075	29.8	0.019
24.2	0.058	22.2	0.069	23.7	0.022
175.1	1.000	175.0	1.000	185.5	1.000
185.7	1.000	185.9	1.000	183.3	0.998
183.6	1.000	183.7	1.000	175.9	0.975
188.1	0.999	188.8	0.999	184.3	0.489
184.4	0.991	184.6	0.997	186.6	0.111
186.7	0.817	187.2	0.964	184.4	0.072
183.3	0.617	183.3	0.943	175.0	0.035

channels evaluated. It means that in each iteration, the number of degrees of freedom for a frequency channel is evaluated over a total of one. This fact makes this method inaccurate, and causes the behavior observed in the figure 3.10 where in temperate climates for the frequencies 175.1 GHz, 185.7 GHz and, 183.6 GHz, and in tropical climates for the frequencies 175.0 GHz, 185.9 GHz, and 183.7 GHz, the degrees of freedom for the signal are practically the same (~ 1, table 3.3). Thus, based on the numbers obtained, for the lower frequencies the optimum chan-

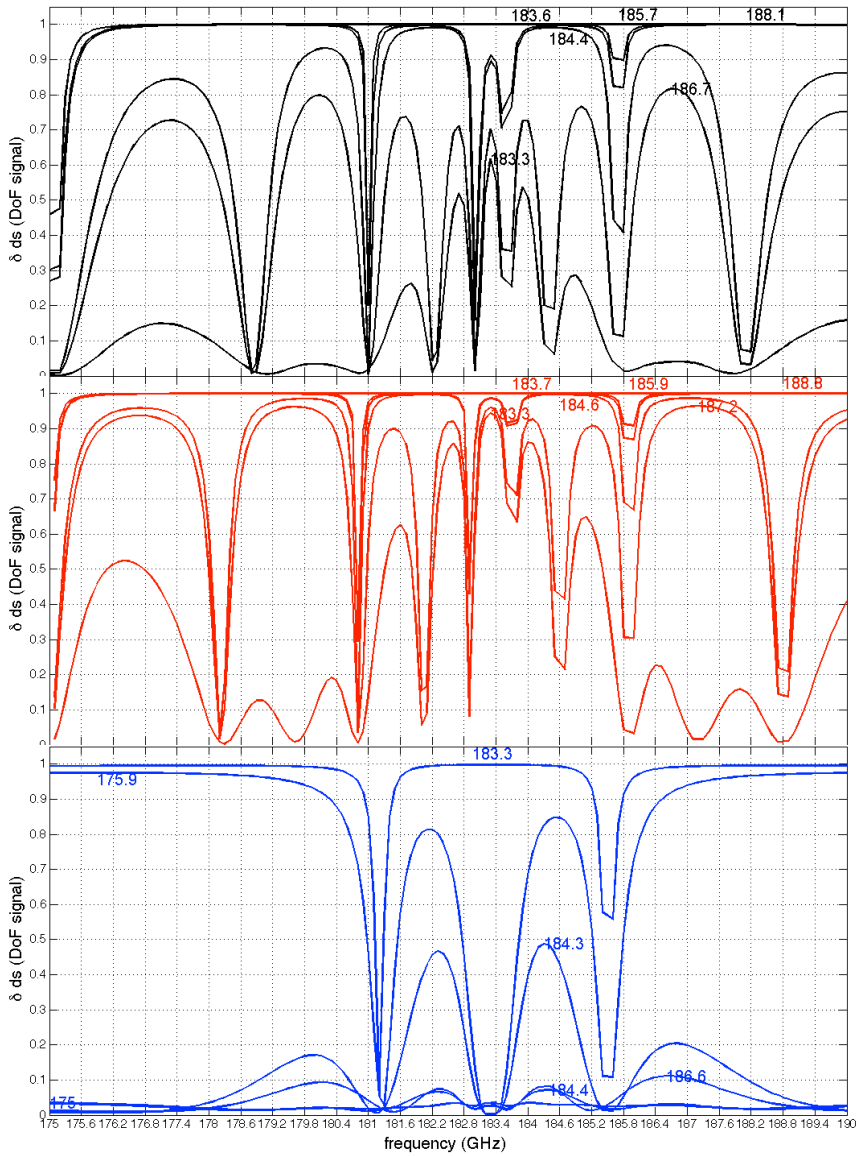

Figure 3.10: Degrees of freedom for high frequency channels and the three climates (2nd iteration)

nels in the tropical climate would be two, while in the temperate and polar climates, only the first channel is the suitable (the second channel has 50% or less number of degrees of freedom than the first one). In case of the higher frequency channels, due to the inaccuracy mentioned before, it is difficult to establish a threshold from where discard correlated channels, meaning that all the channels seem to be presented as the optimum ones.

Otherwise, for the amount of Information Content method in Fig. 3.7 it is clear the amount

of information provided for each channel in each iteration. Numerical values in table 3.2 also denote a clear decrease of the entropy between frequency channels selected in each iteration.

3.4 Channel Selection based on Electrical Path Delay

This method measures the water vapor information retrieved for each frequency channel from the excess electrical path delay (Δ_L), by using the observed upwelling brightness temperature (T_{UP}) from the down looking space borne radiometer.

In figures 3.11 and 3.12 are presented the results for the frequencies around the low (~ 22.235 GHz) and high (~ 183.300 GHz) absorption frequency bands and for the three different climates (temperate, tropical and, polar).

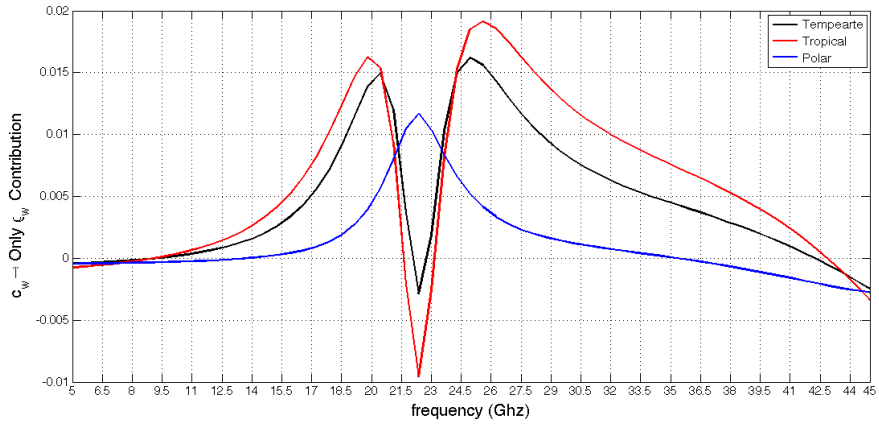

Figure 3.11: Weighted Electrical Path Delay Polynomials for low frequency channels and the three climates

Unlike in the case of the Legendre Polynomials method, as in case of the number of Degrees of Freedom and the amount of Information Content methods, using this method, the resonance frequencies are excluded as the optimum ones to retrieve water vapor information due to the high attenuation along the atmosphere. This fact is clearly observable in the Fig. 3.11, where for temperate and tropical climates there is a mall centered in the resonance frequency (22.235 GHz) while in the tails two peaks can be observed. In case of the polar climates this effect does not take place as the water vapor content in this climate is lower and for this band the absorption is negligible (Figs. 3.2 and 3.3).

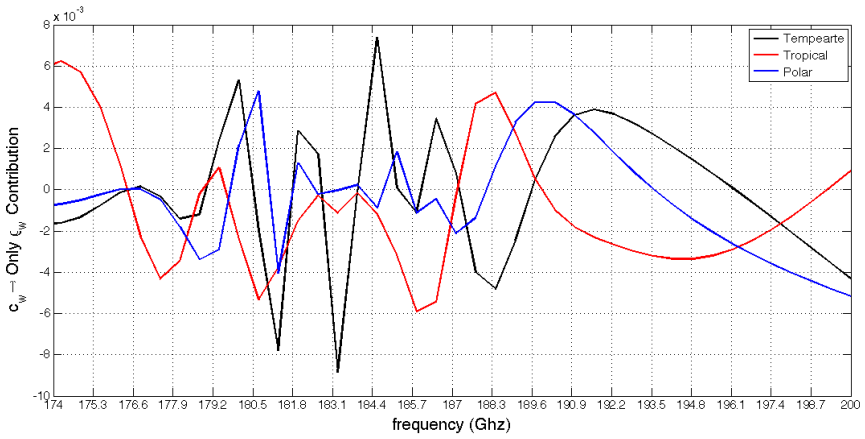

Figure 3.12: Weighted Electrical Path Delay Polynomials for high frequency channels and the three climates

High frequency results are presented in Fig. 3.12, where the observed peaks of contribution less accurate around the absorption band (183.300 GHz), are caused by the high attenuation due to the water vapor content in this band and its rapid variability. From this figure and the numerical results presented in the table 3.4, it can be observed that the more the water vapor content increases in the atmosphere, the selected optimum frequencies more away from the sounding frequency. So in case of the tropical climate, where the water vapor content is around twice higher than in temperate climates, and around twenty times higher than in polar climates (Fig. 2.2) the optimum frequencies are found around 174 GHz and 190 GHz. Otherwise, for polar and temperate climates where the transmissivity is higher (Figs. 3.2 and **??**), frequencies around 180 GHz are considered as the optimum ones.

From this table it can also be observed that the contribution of lower frequencies (~ 24 GHz) is greater than the contribution of higher frequencies (~ 185 GHz). The Electrical Path Delay based method, establish a linear relation between the measured temperature (in this case the upwelling temperature T_{UP}), and the electrical path delay caused by the water vapor content in the atmosphere (ΔL_W). It causes that in zones where there is a high atmospheric water vapor concentration, most attenuated frequencies are interpreted as the ones that are less scattered by the atmospheric water vapor, it is, the ones that have less contribution. This incorrect result is fixed in the iterative methods presented (number of Degrees of Freedom and amount of Information Content based methods), where using the weighting function matrices, the atmospheric profiles evaluated along the atmospheric layers are considered as well .

Table 3.4: Electrical path delay weight for low and high frequency channels and the three climates

Temperate climate		**Tropical climate**		**Polar climate**	
f[GHz]	$c_w(10^{-2})$	**f[GHz]**	$c_w(10^{-2})$	**f[GHz]**	$c_w(10^{-2})$
25.6	1.62	26.2	1.92	23.0	1.17
23.3	1.56	26.8	1.86	22.3	1.05
24.9	1.50	25.6	1.85	23.6	1.03
21.1	1.49	27.5	1.75	24.3	0.83
26.9	1.43	20.4	1.62	21.7	0.79
20.4	1.39	28.1	1.62	24.9	0.66
184.5	0.74	174.2	0.62	180.6	0.48
180.0	0.53	173.6	0.59	189.7	0.42
191.6	0.39	174.9	0.57	190.3	0.42
192.3	0.37	188.4	0.47	190.9	0.36
191.0	0.36	187.7	0.42	189.0	0.33
186.5	0.35	175.5	0.40	191.6	0.28
192.9	0.32	189.0	0.27	180.0	0.21

Methods based on Legendre Polynomials and on the Electrical Path Delay, give different advantages regarding the optimum frequency channel's selection for water vapor retrieval. However, none of them take into account the correlation of the information provided by the different channels. It means that, from selected optimum frequency channels, correlated information, i.e. redundant, could be retrieved.

Iterative channel selection methods (based on the number of Degrees of Freedom and based on the amount of Information Content), consider the information correlation between the selected channels and the remaining ones, improving the results obtained.

3.5 Chanel Selection: The Optimum Method

From the four presented methods, only the method based on the number of Degrees of Freedom and the method based on the amount of Information Content, are able to discard correlated information from the atmosphere. This feature is crucial to get from the minimum number frequency channels (antennas), the best estimation of the water vapor content. On the other hand, the Information Content based method, provides the most accurate results compared to the number of Degrees of Freedom based method, as it measures the change in the atmosphere state entropy in addition to consider uncorrelated information.

Based on the above assumptions, the Information Content based method is the one selected in this project to define the optimum frequency channels, used to correct the excess of electrical path delay, caused by water vapor in coastal zones. As mentioned at the beginning of this report, different climates (temperate, tropical, and polar) are evaluated together with different surfaces (sea, coastal, and ice). The four posed methods were previously evaluated and compared by using the upwelling brightness temperature (T_{UP}), as it contains the main contribution of the state of the atmosphere and gives an overview of all methods without requiring high performance computing.

The results of this method for lower absorption bands and the three climates (temperate, tropical, and polar) are shown in the Figs. 3.13, 3.14, and 3.15 for surface emissivity values of 50%, 75%, and 100% respectively. The same results for higher absorption bands are presented in the Figs. 3.16, 3.17, and 3.18 respectively. These results are based on the brightness temperature defined in Eqn. 2.2.

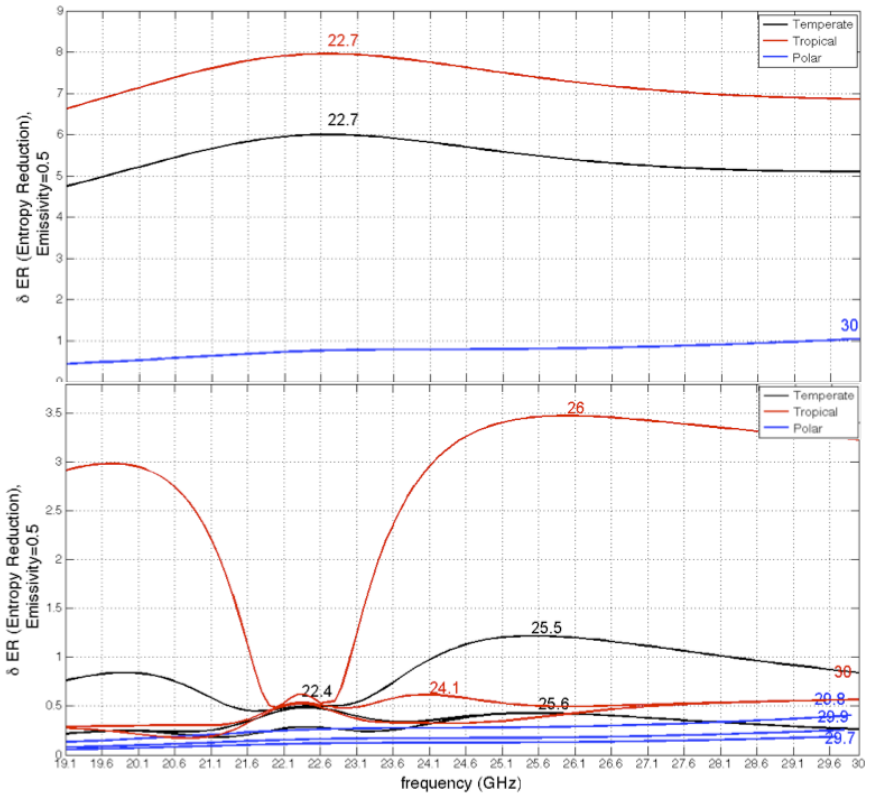

Figure 3.13: Entropy Reduction for lower frequencies, the three climates, and 50% of surface emissivity

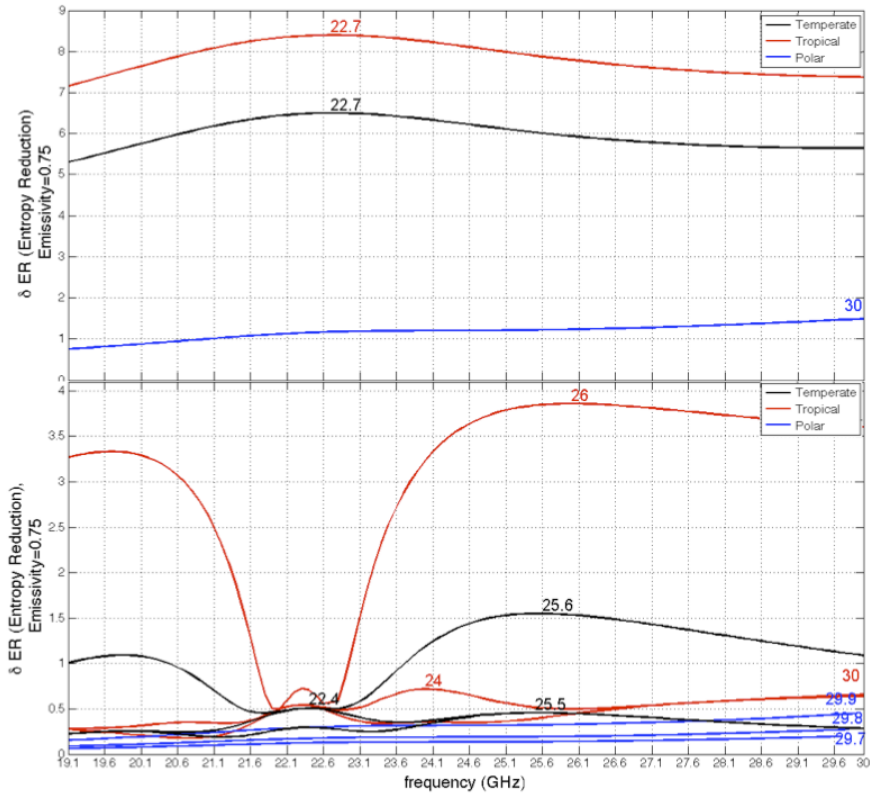

Figure 3.14: Entropy Reduction for lower frequencies, the three climates, and 75% of surface emissivity

In these figures, the first iteration of the method (when the first channel is selected) is shown, and then the following iterations, until a significant number of bits of information it is retained, that in this study the threshold is above 0.2 bits of information. As mentioned previously, resonance frequencies do not turn to be the optimum ones to retrieve information about the state of the atmosphere, as they are strongly affected by the attenuation. In these figures it can be observed that the trend of the information provided does not vary, that means that the optimum frequencies do not change. However, for increasing surface emissivity (from sea $e_s \sim 0.50$ to ice $e_s \sim 1.00$), the information provided by the optimum frequencies also increases. It means that the information given by the surface temperature emitted to the space (T_b) contains more information about the water vapor distribution in the atmosphere than the reflected downwelling temperature (T_{SC}). This is due to the fact that as the upwelling temperature (T_{UP}), the downwelling temperature corresponds to the radiation emitted by the atmosphere as well, so it is expected that the information provided is somewhat similar to the one

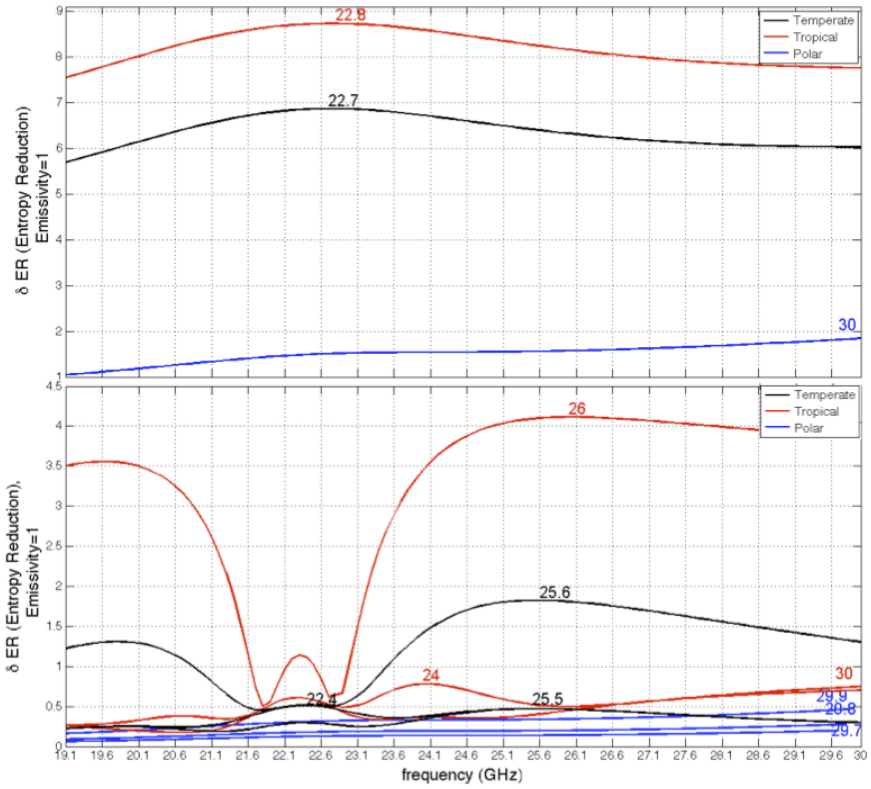

Figure 3.15: Entropy Reduction for lower frequencies, the three climates, and 100% of surface emissivity

provided by the upwelling temperature. In other words, the information is correlated. At lower frequencies, the information provided by the main channels decays rapidly, i.e. one channel provides almost all the information. This fact indicates that the water vapor information provided by lower frequency channels is less affected by the atmospheric gases absorption which is highly correlated, and practically one channel provides most of the information.

Higher resonant frequencies (Figs. 3.16, 3.17, and 3.18) provide actually the largest amount of information on the water vapor for the three climates analyzed. In all cases, the main channels correspond to the three first channels of the higher frequencies. As in the case of the lower resonance frequencies, the tails of the sounding channels are best suited to obtain more information, as they are less affected by gas absorption.

At both high and low resonance frequencies, the distribution of the information between the remaining channels has a common behavior everytime a channel is selected. Each time a channel is selected, the information of the remaining channels is reevaluated, discarding those

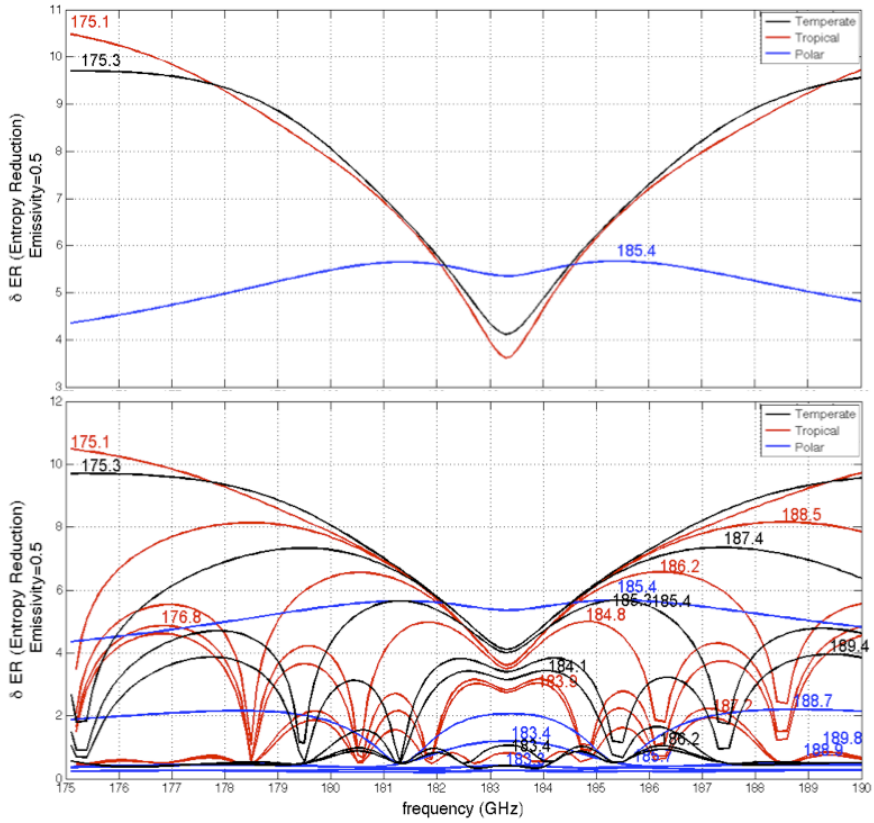

Figure 3.16: Entropy Reduction for higher frequencies, the three climates, and 50% of surface emissivity

channels that provide information correlated to the information already provided with the selected ones. Since the main channels are at the tails of the resonance frequencies, it can be observed that after the 3^{th} or 4^{th} iteration, the channels containing most information start getting closer to the resonant frequencies. This indicates that the tails are less attenuated, but more correlated among them in terms of amount of information. This effect is clearly visible for the high resonance frequencies in tropical climates. Tables 3.5, 3.6, and 3.7 show in detail these results numerically.

Finally, Fig. 3.21 presents the weighting functions (Eqn. 2.7) for the main frequency channels of each climate and surface emissivity. As it can be seen, the first four channels contain information on the water vapor in the troposphere up to $\sim 5-7$ km for temperate and tropical climates, and up to $\sim 3-4$ km for polar climates. These figures gives also a clear view of the impact of the surface emissivity on the sensibility of the brightness temperature to the atmo-

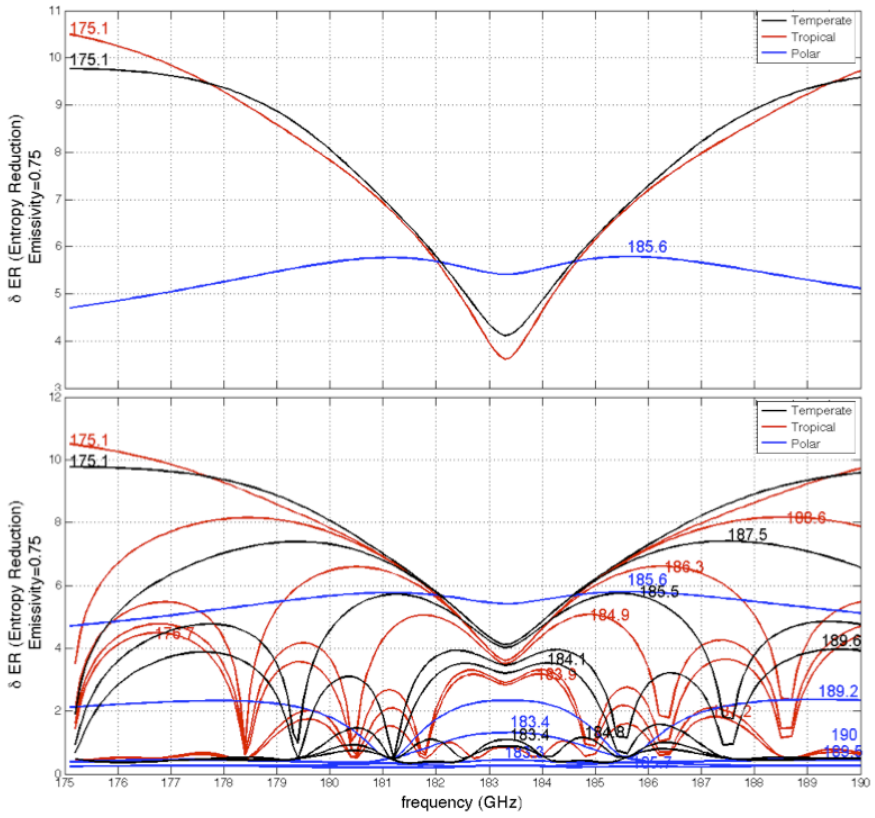

Figure 3.17: Entropy Reduction for higher frequencies, the three climates, and 75% of surface emissivity

spheric water vapor. As previously discussed, the increase of the surface emissivity augments the presence of the surface temperature (T_b) into the observations that contains important information on the variability of the water vapor in lower layers of the troposphere, and it is more uncorrelated to the upwelling brightness temperature (T_{UP}) than the reflected downwelling brightness temperature (T_{SC}). This effect can be observed through the polar climates, where there is lower concentration of the water vapor in the troposphere. In Fig. 3.21, it can be observed for this climate that a frequency channel at 184.4 GHz provides the largest amount of information from the lower troposphere when the surface emissivity is increased. This fact enhances the presence of the surface temperature (T_b) into the retrieved brightness temperature (T_B), that as explained previously is less correlated with the atmospheric radiated temperatures (T_{DN}, and T_{UP}), so that provides more information about the water vapor distribution.

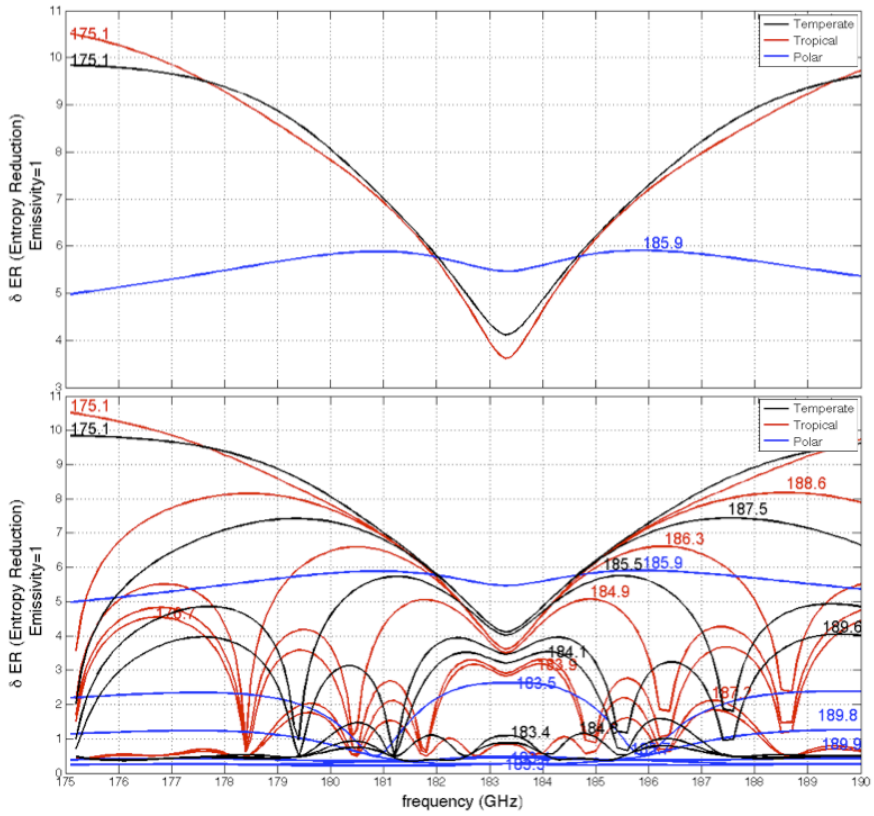

Figure 3.18: Entropy Reduction for higher frequencies, the three climates, and 100% of surface emissivity

Table 3.5: Entropy reduction for low and high frequency channels: temperate climate

Surface's emissivity $e_s = 0.50$		**Surface's emissivity $e_s = 0.75$**		**Surface's emissivity $e_s = 1.00$**	
f[GHz]	**ER[bits]**	**f[GHz]**	**ER[bits]**	**f[GHz]**	**ER[bits]**
22.7	6.001	22.7	6.498	22.7	6.868
25.5	1.220	25.6	1.550	25.6	1.824
22.4	0.486	22.4	0.503	22.4	0.513
25.6	0.429	25.5	0.456	25.5	0.471
22.5	0.286	22.3	0.292	22.3	0.296
25.7	0.267	25.7	0.277	25.7	0.282
22.3	0.204	22.5	0.207	25.5	0.208
175.3	9.700	175.1	9.769	175.1	9.837
187.4	7.349	187.5	7.405	187.5	7.437
185.4	5.672	185.5	5.735	185.5	5.751
189.4	3.952	189.6	3.964	189.6	4.050
184.1	3.435	184.1	3.531	184.1	3.535
183.4	1.054	184.8	1.158	184.8	1.162
186.2	0.935	183.4	0.877	183.4	0.877

Table 3.6: Entropy reduction for low and high frequency channels: tropical climate

Surface's emissivity $e_s = 0.50$		**Surface's emissivity $e_s = 0.75$**		**Surface's emissivity $e_s = 1.00$**	
f[GHz]	**ER[bits]**	**f[GHz]**	**ER[bits]**	**f[GHz]**	**ER[bits]**
22.7	7.957	22.7	8.395	22.8	8.732
26.0	3.474	26.0	3.858	26.0	4.115
24.1	0.618	24.0	0.716	24.0	0.779
30.0	0.567	30.0	0.639	30.0	0.704
22.3	0.526	22.3	0.537	22.3	0.595
24.2	0.326	24.2	0.351	24.2	0.361
29.9	0.312	29.9	0.331	29.9	0.344
175.1	10.480	175.1	10.496	175.1	10.511
188.5	8.158	188.6	8.166	188.6	8.174
186.2	6.573	186.3	6.607	186.3	6.611
184.8	4.993	184.9	5.069	184.9	5.071
176.8	4.609	176.7	4.489	176.7	4.544
183.9	3.037	183.9	3.177	183.9	3.179
187.2	1.937	187.2	1.823	187.2	1.838

Table 3.7: Entropy reduction for low and high frequency channels: polar climate

Surface's emissivity e_s = 0.50		**Surface's emissivity e_s = 0.75**		**Surface's emissivity e_s = 1.00**	
f[GHz]	**ER[bits]**	**f[GHz]**	**ER[bits]**	**f[GHz]**	**ER[bits]**
30.0	1.047	30.0	1.491	30.0	1.844
29.9	0.405	29.9	0.448	29.9	0.467
29.8	0.255	29.8	0.271	29.8	0.278
185.4	5.670	185.6	5.787	185.9	5.905
188.7	2.198	189.2	2.366	183.5	2.631
183.4	1.190	183.4	1.315	189.8	1.258

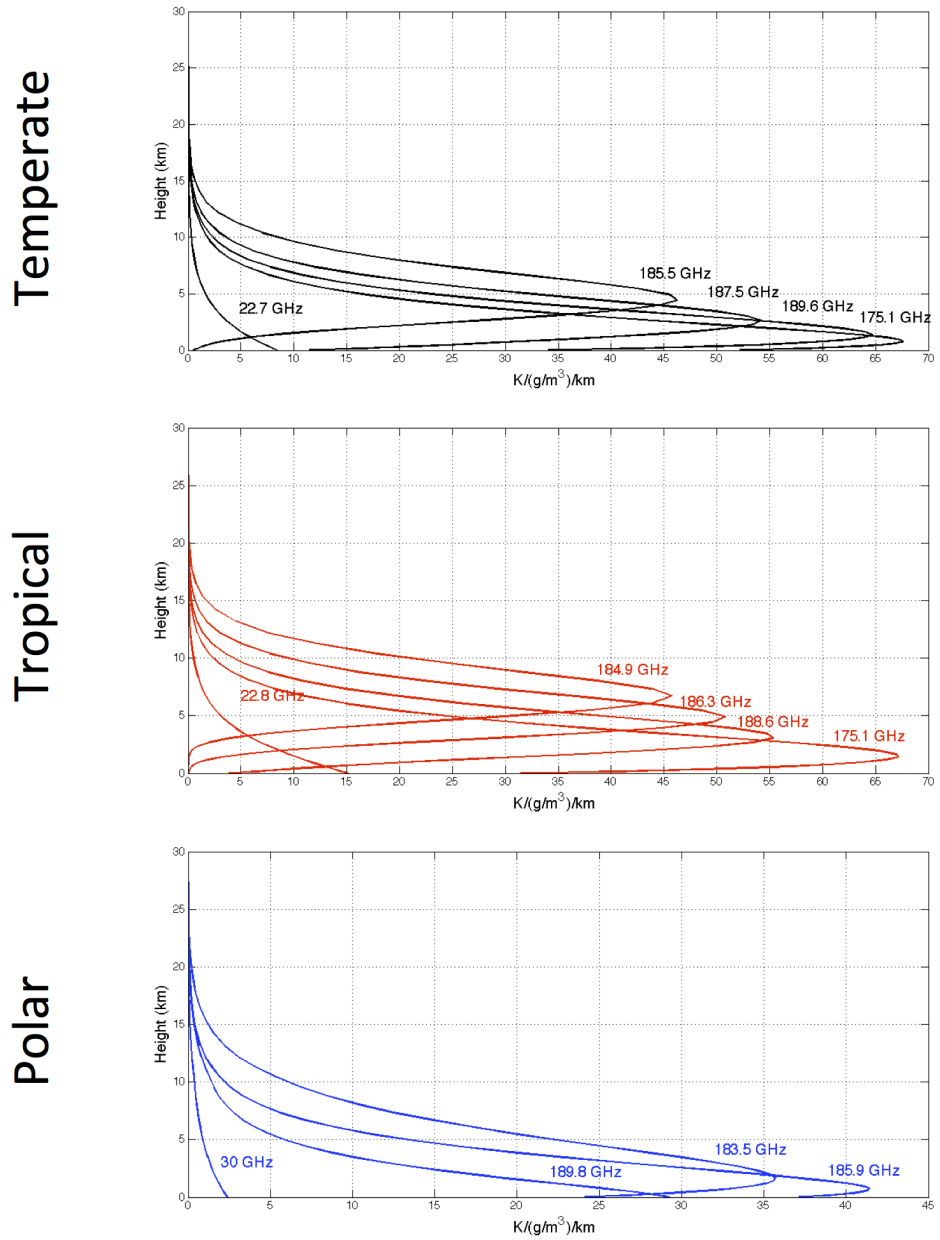

Figure 3.19: Water vapor optimum channels' Weighting Functions with 50% of surface emissivity

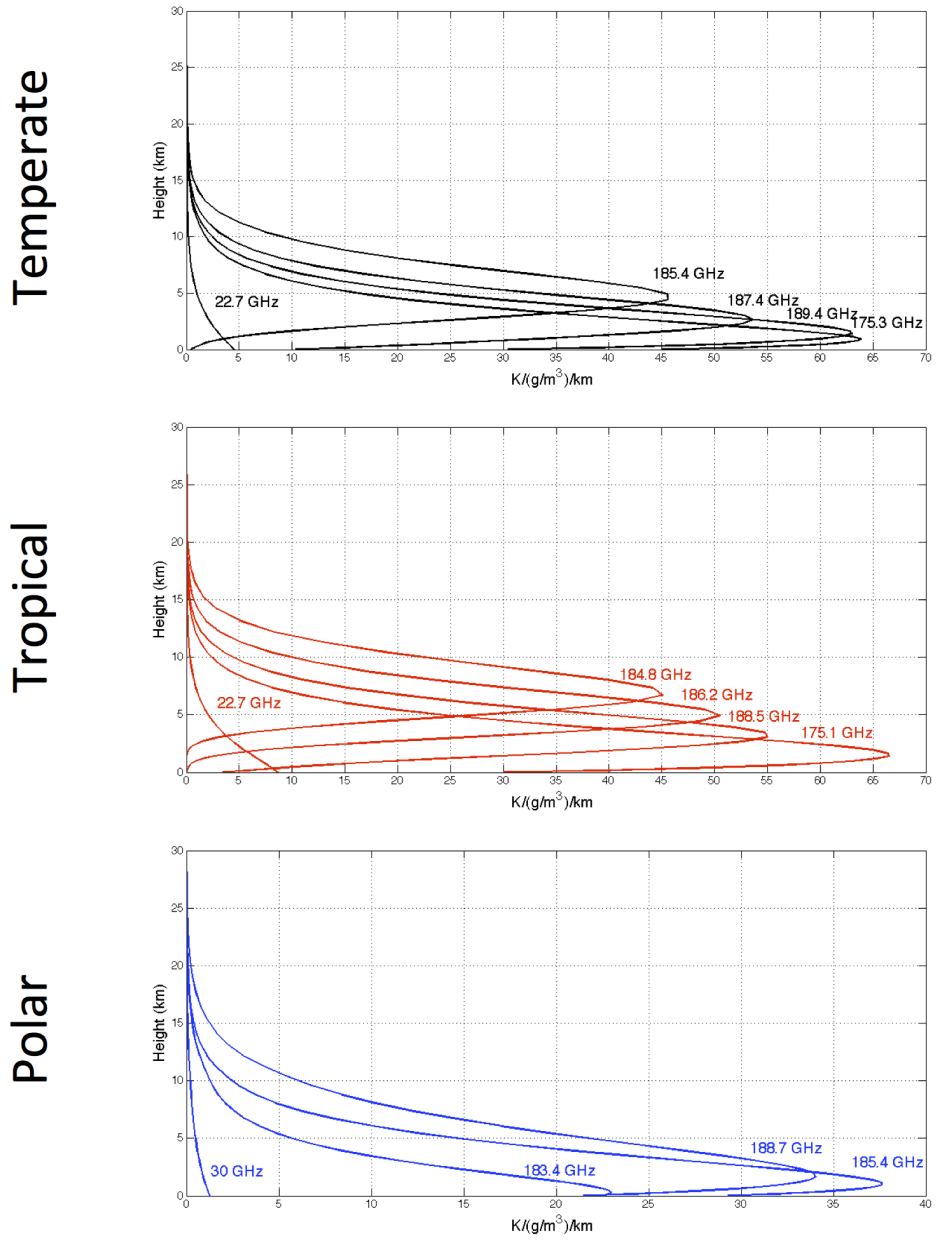

Figure 3.20: Water vapor optimum channels' Weighting Functions with 75% of surface emissivity

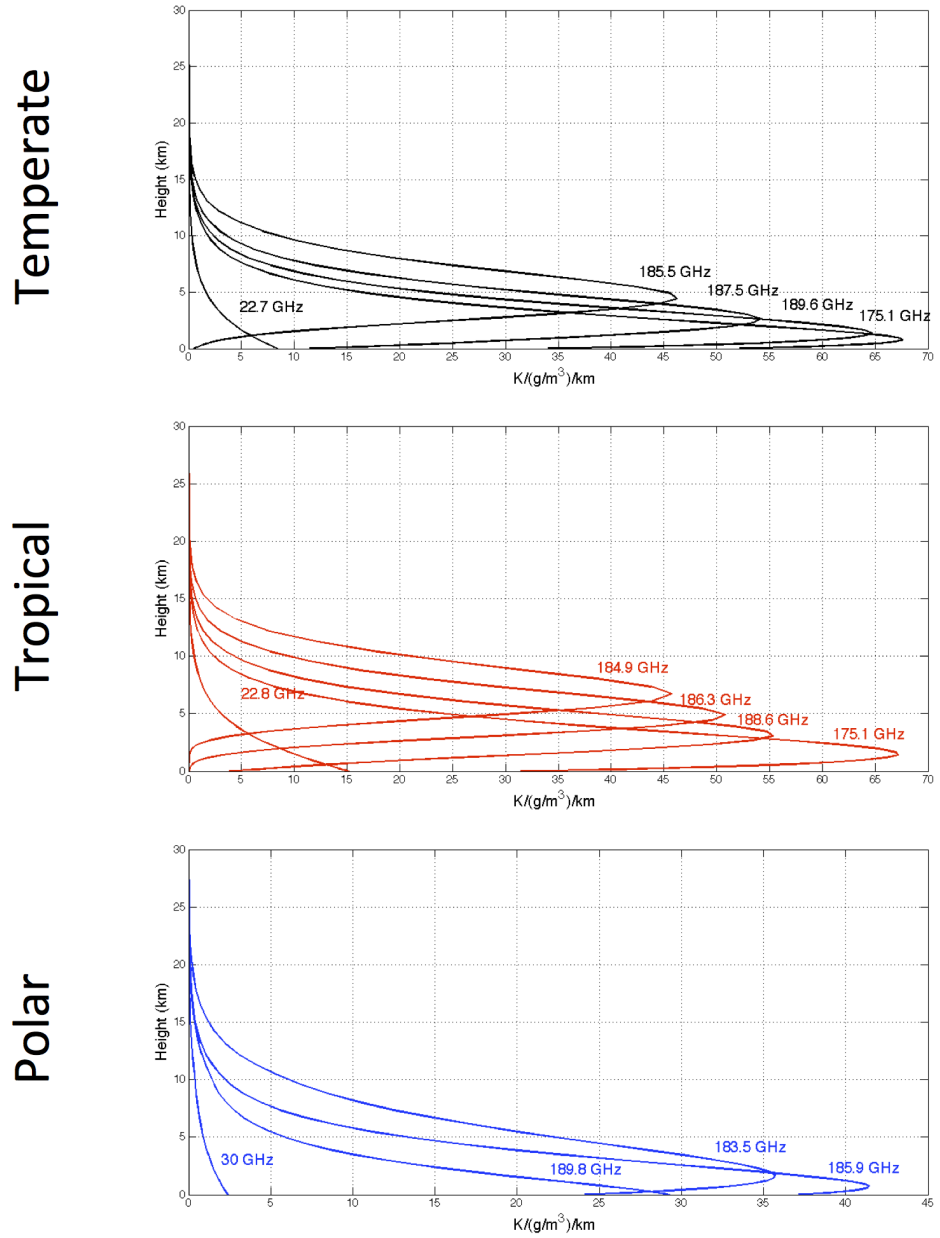

Figure 3.21: Water vapor optimum channels' Weighting Functions with 100% of surface emissivity

CHAPTER 4

WET ELECTRICAL PATH DELAY ACCURACY

Once the optimum frequency channels are defined, the accuracy of the excess electrical path delay estimation is calculated in this chapter. This accuracy is calculated from Eqn. 4 as the impact of the noise in the observed brightness temperature for each frequency channel selected

$$\sigma^2_{\Delta L_W} = \sum_{i=1}^{N} c_i^2 \cdot \Delta T^2_{B_i}, \tag{4.1}$$

where c_i is the weight of the measured brightness temperature in the excess electrical path delay caused by the water vapor Δ_{L_W}, and is calculated as explained in Eqn. 2.69 for 100 simulated scenarios or atmospheric conditions, i.e. each ΔL_W is the result of the combination of 100 brightness temperatures (T_B) retrieved in 100 different atmospheric conditions for the three different climates (temperate, tropical, and polar) and the three different surfaces (sea, coastal, and ice).

So, for a combination of channels, it is got the variance on the excess electrical path delay depending on the noise of the observations. In case the error in the measurements is uncorrelated, the variance of the excess electrical path delay Δ_{L_W} is negligible, meaning that the set of channels are suitable for noisy environments, otherwise , the result indicates a lower accuracy against the signal error.

Tables 4.1, 4.2, and 4.3 present the results obtained for the three climates (temperate, trop-

ical, and polar) considering the optimum frequency channels for the three different surfaces (sea, coastal, and ice), when there is noise present in the brightness temperature observations (T_B). The standard deviation of the excess electrical path delay ($\sigma^2_{\Delta L_W}$) is calculated for each particular set of frequencies when there is presence of noise in one of the channels. The set of frequency channels used in this chapter, correspond for the lower frequencies to the first two optimum channels obtained in the previous chapter (note that in case of the polar climates, the second channel provides less than one bit of information). For higher frequencies, the channels used correspond to the first four channels obtained in the previous chapter for the temperate and tropical climates, and to the three channels obtained for polar climates.

In the table 4.1 for the temperate climate, it can be observed that the most inaccurate frequencies are located in lower absorption bands (around ~ 24.0 GHz) for 100% of surface emissivity ($e_s = 1$). As an example, for the frequency 25.6 GHz in high emissivity surface just 0.1 Kelvin degree of noise in the measure would cause a deviation in the electrical path delay estimation of ~ 36 cm, which is useless.

This behavior is common for the three analyzed climates, where the more the surface emissivity increases, the larger the noise. As explained in the previous chapter when the surface emissivity increases, the presence of the surface brightness temperature in the measured brightness temperature (T_B) also increases. This emitted temperature, provides more information about water vapor distribution in the atmosphere, cause referring to the atmospheric water vapor profile (Fig. 2.2), the major part of its concentration is found below the 10 km, i.e. in the troposphere. This fact may cause that added noise in the observation frequency channels over an ice surface, has a larger impact in the estimated electrical path delay, while in zones where the contribution of surface emitted brightness temperature (T_b) is lower, the presence of noise in the observation frequency channels has a lower impact.

Another notable feature from the three tables is that it is not possible to define the same trend of attenuation in terms of frequency channels for the different climates, as an example, for tropical climates over high emissivity surfaces, the channels that are more affected by the added noise are those ones from the higher absorption bands. On the other hand, in case of temperate and polar climates, and for the high emissivity surfaces, the optimum channels in presence of noise are the lower frequency ones.

Table 4.1: Electrical Path Delay error in temperate climates

Surface's emissivity $e_s = 0.50$			**Surface's emissivity $e_s = 0.75$**			**Surface's emissivity $e_s = 1.00$**		
f [GHz]	**$\Delta T_B[K]$**	**$\lvert\sigma_{\Delta L_W}\rvert[m]$**	**f [GHz]**	**$\Delta T_B[K]$**	**$\lvert\sigma_{\Delta L_W}\rvert[m]$**	**f [GHz]**	**$\Delta T_B[K]$**	**$\lvert\sigma_{\Delta L_W}\rvert[m]$**
$c_W = 0.134$			**$c_W = 0.378$**			**$c_W = -3.24$**		
22.7	0.1	0.013	22.7	0.1	0.038	22.7	0.1	0.324
22.7	0.2	0.027	22.7	0.2	0.076	22.7	0.2	0.648
22.7	0.3	0.040	22.7	0.3	0.114	22.7	0.3	0.972
22.7	0.4	0.053	22.7	0.4	0.151	22.7	0.4	1.300
$c_W = -0.152$			**$c_W = -0.275$**			**$c_W = 3.67$**		
25.5	0.1	0.015	25.6	0.1	0.028	25.6	0.1	0.367
25.5	0.2	0.030	25.6	0.2	0.055	25.6	0.2	0.735
25.5	0.3	0.046	25.6	0.3	0.083	25.6	0.3	1.102
25.5	0.4	0.061	25.6	0.4	0.110	25.6	0.4	1.470
$c_W = 0.154$			**$c_W = 0.236$**			**$c_W = -1.805$**		
175.3	0.1	0.015	175.1	0.1	0.024	175.1	0.1	0.181
175.3	0.2	0.031	175.1	0.2	0.047	175.1	0.2	0.361
175.3	0.3	0.046	175.1	0.3	0.071	175.1	0.3	0.542
175.3	0.4	0.062	175.1	0.4	0.094	175.1	0.4	0.722
$c_W = 0.148$			**$c_W = 0.336$**			**$c_W = -1.028$**		
187.4	0.1	0.015	187.5	0.1	0.034	187.5	0.1	0.103
187.4	0.2	0.030	187.5	0.2	0.070	187.5	0.2	0.206
187.4	0.3	0.044	187.5	0.3	0.101	187.5	0.3	0.308
187.4	0.4	0.060	187.5	0.4	0.134	187.5	0.4	0.411
$c_W = 0.043$			**$c_W = -0.200$**			**$c_W = 0.154$**		
185.4	0.1	0.004	185.5	0.1	0.020	185.5	0.1	0.015
185.4	0.2	0.009	185.5	0.2	0.040	185.5	0.2	0.031
185.4	0.3	0.013	185.5	0.3	0.060	185.5	0.3	0.046
185.4	0.4	0.017	185.5	0.4	0.080	185.5	0.4	0.062
$c_W = 0.233$			**$c_W = -0.430$**			**$c_W = 2.246$**		
189.4	0.1	0.023	189.6	0.1	0.043	189.6	0.1	0.225
189.4	0.2	0.047	189.6	0.2	0.086	189.6	0.2	0.449
189.4	0.3	0.070	189.6	0.3	0.130	189.6	0.3	0.673
189.4	0.4	0.093	189.6	0.4	0.172	189.6	0.4	0.898

Table 4.2: Electrical Path Delay error in tropical climates

Surface's emissivity $e_s = 0.50$			**Surface's emissivity $e_s = 0.75$**			**Surface's emissivity $e_s = 1.00$**		
f [GHz]	**$\Delta T_B[K]$**	**$\lvert\sigma_{\Delta L_W}\rvert[m]$**	**f [GHz]**	**$\Delta T_B[K]$**	**$\lvert\sigma_{\Delta L_W}\rvert[m]$**	**f [GHz]**	**$\Delta T_B[K]$**	**$\lvert\sigma_{\Delta L_W}\rvert[m]$**
$c_W = 0.061$			**$c_W = 0.080$**			**$c_W = -2.692$**		
22.7	0.1	0.006	22.7	0.1	0.008	22.8	0.1	0.269
22.7	0.2	0.012	22.7	0.2	0.016	22.8	0.2	0.538
22.7	0.3	0.018	22.7	0.3	0.024	22.8	0.3	0.808
22.7	0.4	0.025	22.7	0.4	0.032	22.8	0.4	1.077
$c_W = 0.032$			**$c_W = 0.520$**			**$c_W = 3.127$**		
26.0	0.1	0.032	26.0	0.1	0.052	26.0	0.1	0.312
26.0	0.2	0.065	26.0	0.2	0.104	26.0	0.2	0.625
26.0	0.3	0.097	26.0	0.3	0.156	26.0	0.3	0.938
26.0	0.4	0.130	26.0	0.4	0.208	26.0	0.4	1.250
$c_W = -0.028$			**$c_W = -0.07$**			**$c_W = -1.801$**		
175.1	0.1	0.003	175.1	0.1	0.008	175.1	0.1	0.180
175.1	0.2	0.006	175.1	0.2	0.015	175.1	0.2	0.360
175.1	0.3	0.008	175.1	0.3	0.022	175.1	0.3	0.540
175.1	0.4	0.011	175.1	0.4	0.030	175.1	0.4	0.720
$c_W = 0.078$			**$c_W = 0.266$**			**$c_W = 7.848$**		
188.5	0.1	0.008	188.6	0.1	0.027	188.6	0.1	0.785
188.5	0.2	0.016	188.6	0.2	0.053	188.6	0.2	1.570
188.5	0.3	0.023	188.6	0.3	0.080	188.6	0.3	2.354
188.5	0.4	0.031	188.6	0.4	0.106	188.6	0.4	3.140
$c_W = -0.460$			**$c_W = -2.369$**			**$c_W = -12.442$**		
186.2	0.1	0.046	186.3	0.1	0.237	186.3	0.1	1.244
186.2	0.2	0.092	186.3	0.2	0.474	186.3	0.2	2.489
186.2	0.3	0.138	186.3	0.3	0.711	186.3	0.3	3.733
186.2	0.4	0.184	185.5	0.4	0.947	186.3	0.4	4.977
$c_W = 0.271$			**$c_W = 1.832$**			**$c_W = -5.985$**		
184.8	0.1	0.027	184.9	0.1	0.183	184.9	0.1	0.599
184.8	0.2	0.054	184.9	0.2	0.366	184.9	0.2	1.197
184.8	0.3	0.081	184.9	0.3	0.550	184.9	0.3	1.796
184.8	0.4	0.109	184.9	0.4	0.733	184.9	0.4	2.394

Table 4.3: Electrical Path Delay error in polar climates

Surface's emissivity $e_s = 0.50$			**Surface's emissivity $e_s = 0.75$**			**Surface's emissivity $e_s = 1.00$**		
f [GHz]	**$\Delta T_B[K]$**	**$\lvert\sigma_{\Delta L_W}\rvert[m]$**	**f [GHz]**	**$\Delta T_B[K]$**	**$\lvert\sigma_{\Delta L_W}\rvert[m]$**	**f [GHz]**	**$\Delta T_B[K]$**	**$\lvert\sigma_{\Delta L_W}\rvert[m]$**
$c_W = -88.147$			**$c_W = -195.143$**			**$c_W = 42.586$**		
30.0	0.1	8.814	30.0	0.1	19.514	30.0	0.1	4.259
30.0	0.2	17.629	30.0	0.2	39.029	30.0	0.2	8.517
30.0	0.3	26.444	30.0	0.3	58.542	30.0	0.3	12.776
30.0	0.4	35.259	30.0	0.4	78.057	30.0	0.4	17.034
$c_W = 88.199$			**$c_W = 195.1699$**			**$c_W = -42.377$**		
29.9	0.1	8.820	29.9	0.1	19.517	29.9	0.1	4.238
29.9	0.2	17.640	29.9	0.2	39.034	29.9	0.2	8.476
29.9	0.3	26.460	29.9	0.3	58.551	29.9	0.3	12.713
29.9	0.4	35.280	29.9	0.4	78.068	29.9	0.4	16.951
$c_W = -0.1 \cdot 10^{-3}$			**$c_W = 0.2 \cdot 10^{-3}$**			0.018		
185.4	0.1	$7.038 \cdot 10^{-6}$	185.6	0.1	$1.906 \cdot 10^{-5}$	185.9	0.1	0.002
185.4	0.2	$1.407 \cdot 10^{-5}$	185.6	0.2	$3.813 \cdot 10^{-5}$	185.9	0.2	0.004
185.4	0.3	$2.112 \cdot 10^{-5}$	185.6	0.3	$5.720 \cdot 10^{-5}$	185.9	0.3	0.005
185.4	0.4	$2816 \cdot 10^{-5}$	185.6	0.4	$7.626 \cdot 10^{-5}$	185.9	0.4	0.007
$c_W = 0.004$			**$c_W = 0.010$**			**$c_W = -0.1 \cdot 10^{-4}$**		
188.7	0.1	$3.681 \cdot 10^{-4}$	189.2	0.1	$9.570 \cdot 10^{-4}$	183.5	0.1	$1.154 \cdot 10^{-5}$
188.7	0.2	$7.361 \cdot 10^{-4}$	189.2	0.2	0.002	183.5	0.2	$2.308 \cdot 10^{-5}$
188.7	0.3	0.001	189.2	0.3	0.003	183.5	0.3	$3.462 \cdot 10^{-5}$
188.7	0.4	0.002	189.2	0.4	0.0040	183.5	0.4	$4.616 \cdot 10^{-5}$
$c_W = 0$			**$c_W = 0$**			**$c_W = -0.226$**		
183.4	0.1	$2.522 \cdot 10^{-8}$	183.4	0.1	$3.841 \cdot 10^{-8}$	189.8	0.1	0.0223
183.4	0.2	$5.044 \cdot 10^{-8}$	183.4	0.2	$7.682 \cdot 10^{-8}$	189.8	0.2	0.045
183.4	0.3	$7.567 \cdot 10^{-8}$	183.4	0.3	$1.152 \cdot 10^{-7}$	189.8	0.3	0.068
183.4	0.4	$1.009 \cdot 10^{-7}$	183.4	0.4	$1.536 \cdot 10^{-7}$	189.8	0.4	0.090

Finally, based on an expected accuracy of 2 cm, from the values obtained in the previous chapter, and considering influence of noise in the measurements, the suitable channels for each climate are presented in the tables 4.4, 4.5, and 4.6.

Table 4.4: Optimum frequency Channels for temperate climates

Temperate climates		
Frequency [GHz]	**Surface emissivity**	**Noise [K]**
22.7	50%	0.1
25.5	50%	0.1
175.3	50%	0.1
187.4	50%	0.1
185.4	50%	0.4

Table 4.5: Optimum frequency Channels for tropical climates

Tropical climates		
Frequency [GHz]	**Surface emissivity**	**Noise [K]**
22.7	50%	0.3
	75%	0.2
175.1	50%	0.4
	75%	0.2
188.5	50%	0.2

Table 4.6: Optimum frequency Channels for polar climates

Polar climates		
Frequency [GHz]	**Surface emissivity**	**Noise [K]**
185.4	50%	0.4
	75%	0.4
	100%	0.4
188.7	50%	0.4
	75%	0.4
	100%	0.4
183.4	50%	0.4
	75%	0.4

CHAPTER 5

CONCLUSIONS AND FUTURE RESEARCH

The number of channels to be included in a radiometer instrument will be ultimately dictated by: 1) the achievable accuracy of the water vapor correction for a given number of frequency channels and associated radiometric errors (both radiometric accuracy or systematic errors, and a radiometric sensitivity of random errors), and 2) the instrument complexity and cost.

From results obtained in the Chapter 3, in the high frequency band the channels that provide the largest amount of information are 175.1 GHz, ~ 188.1 GHz, and ~ 185.5 GHz for temperate climates, 175.1 GHz, ~ 188.5 GHz, and ~ 183.5 GHz for tropical climates, and ~ 185.5 GHz, 189.2 GHz, and 183.5 GHz for polar climates, while in the lower frequency bands the optimum channels are: 22.7 GHz, and 25.5 GHz for the temperate climates, 22.7 GHz, and 26.0 GHz for tropical climates, and around 30 GHz for polar climates. These frequency channels are quite similar for tropical and temperate climates, but differ for polar climates.

On the other hand, channels of lower resonance frequencies are more sensitive to changes in the surface's emissivity must be included, as they are very sensitive to the variability of water vapor in coastal zones.

However, a much better spatial resolution can be achieved using the higher frequency channels, as compared to the low frequency channels, for the same antenna size.

In the Chapter 3, the results obtained are based on a noise free frequency channels. The noise impact is evaluated in the Chapter 4, where to a set of channels it is applied an error

in the measurements. Depending on the climate and surface, the impact of this error causes that most of the presented as optimum frequency channels, need to be discarded as they do not fulfill the accuracy required. Then from six evaluated channels in temperate and tropical climates, six can be used over sea surfaces in temperate climates, three over sea surfaces in tropical climates and two over coastal surfaces in tropical climates as well. In polar climates, from five analyzed channels, just three (higher frequencies) remain as optimum to be used over the three surfaces (sea, coastal, and ice).

These results does not seem to be following a common trend, making necessary to investigate further from all channels that provide information about the atmosphere state (based on the bits of entropy), all the possible combinations of climate, surface, frequency, and noise, that lead to an optimal result.

Future research lines of this study will extend the range of frequencies ($f > 200$ GHz), and will consider the atmospheric scattering by hydrometeors. On the other hand, this study is based on simulated results on ideal scenarios, where the water vapor distribution is a perfect exponential function. Thus in order to improve results obtained in this study, real data measured in different climates, for different pressure levels and surfaces, and considering also different year seasons needs to be introduced in the calculations done.

APPENDIX

ANNEX

ON THE AMOUNT OF INFORMATION CONTENT IN MICROWAVE RADIOMETRY FOR WET DELAY ESTIMATION

Journal:	*Journal of Selected Topics in Applied Earth Observations and Remote Sensing*
Manuscript ID	JSTARS-2016-00575
Manuscript type:	MicroRad 2016
Date Submitted by the Author:	29-Jun-2016
Complete List of Authors:	Gual de Torrella, Jose; Universitat Politecnica de Catalunya, Dept. of Signal Theory and Communications Camps, Adriano; Polytechnic University of Catalonia, Dept of Signal Theory and COmmunications; IEEC, CRAE/UPC
Keywords:	Water, Atmospheric measurements, Radar altimetry, Radiometry, Entropy, Delay effects

ON THE AMOUNT OF INFORMATION CONTENT IN MICROWAVE RADIOMETRY FOR WET DELAY ESTIMATION

J. Gual and A. Camps

Remote Sensing Lab, Dept. of Signal Theory and Communications
Universitat Politècnica de Catalunya-Barcelona Tech and IEEC/CTE-UPC
UPC Campus Nord, building D4, 08034 Barcelona, Spain,
e-mail: jmgualcovas@gmail.com, camps@tsc.upc.edu

ABSTRACT

This work aims at determining the set of optimum frequencies to be used in the companion microwave radiometers in future synthetic aperture radar altimeters, to provide higher spatial resolution of the atmospheric water vapor state so as to improve the wet delay correction in coastal regions. The channel selection is based on the study of the frequencies that provide the largest amount of information, as defined by the largest information entropy change from a prior knowledge state. It is found that four frequencies, one close to the 22 GHz peak, and three other ones around 175.188 GHz provide a near optimum compromise between the amount of information measured, and the instrument's complexity.

Index Terms—wet delay, atmospheric water vapor, microwave radiometer, radar altimeter, weighting functions, entropy, information content.

1. INTRODUCTION

Satellite altimetry plays an important role among the Earth observation techniques, and it is very useful for ocean missions. *Coastal Altimetry* (approximately 0-50 km away from the coast), allows to study storm surge's by measuring the Total Water Level Envelope (TWLE), and it is also very useful in wave models. However, coastal altimetry data is inaccurate and difficult to interpret due to the variation of the waveforms' shape (shape of the radar returns), when the antenna footprint of the instrument enters in the land, and because of the rapid variations of the wet tropospheric delay. The application of SAR techniques to radar altimetry, such as in ESA's CryoSat-2 mission has allowed to significantly improve the along-track resolution, providing much better results than in pulse-limited altimeters. Nevertheless for these high-resolution altimeters, an optimized delay correction is needed to solve the rapid tropospheric wet delay variability [1].

In this study a methodology is presented to identify from the measured brightness temperature of the atmosphere, a set of frequency channels that provide the most significant and uncorrelated information on the water vapor content in the atmosphere.

First of all a Mathematic model is defined to describe the Physics of the atmosphere, and from this model the contribution of the water vapor into the brightness temperatures as measured by a nadir-looking microwave radiometer are derived. Then, a Mathematical model using inversion methods to select frequency channels providing the largest amount of data (i.e. uncorrelated data) is defined. Finally, results for three "standard" climates (tropical, temperate, and polar) are presented. Synthetic atmospheric pressure, temperature, and water vapor profiles are used, and different surface emissivities are also considered in the computation of the down-looking brightness temperatures for the three atmosphere models.

2. METHODOLOGY

2.1. Forward Model

In this study three different atmosphere models are considered for the three different climates: tropical, temperate, and polar, and for the three different types of surfaces: ice, sea, and coastal regions. The three standard atmosphere models are generated using as input parameters the water vapor, temperature, and pressure from 0 km (sea surface height), up to 64 km height (mesosphere). The atmospheric temperature, pressure, and water vapor profiles ($T(z)$, $P(z)$, and $\rho_v(z)$) for the three different climates are described in [2, pp. 339-373] (Fig. 1), and they are used to compute the gas absorption ($\kappa_\alpha(f,z)$) as a function of the frequency and height, the atmospheric optical thickness ($\tau(z,\infty)$), the upwelling temperature (T_{UP}), and downwelling temperature (T_{DN}) as a function of the frequency (f). Finally, three different surface emissivitie are used to calculate the surface brightness temperature (T_b), and the downwelling temperature reflected back to the atmosphere (T_{sc}).

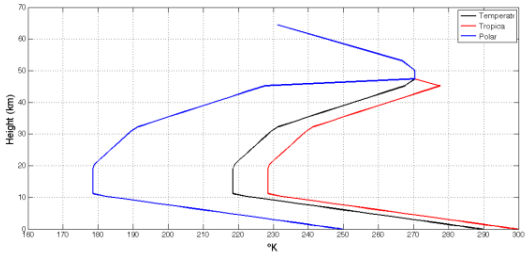

a)

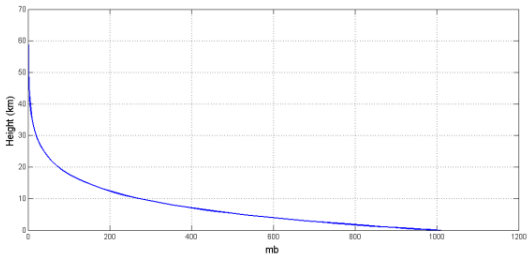

b)

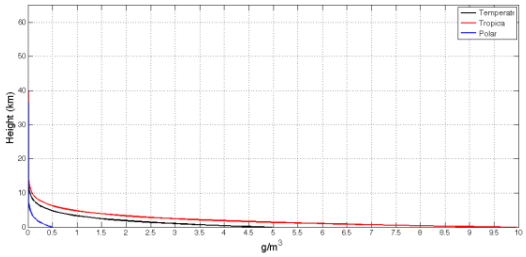

c)

Fig. 1. Atmospheric temperature, pressure, and water vapor profiles used for the three climate models.

The emissivity values are 1.00, 0.50 and 0.75, which correspond approximately to those of the ice, ocean, and coastal regions, respectively. Finally, the brightness temperature reaching the radiometer antenna (T_B, Eqn. 1) is then computed for the nine possible combinations of the three different climates and the three different surfaces:

$$T_B = T_{UP} + (T_b + T_{SC}) \cdot e^{-\tau(0,\infty)}, \quad (1)$$

$$T_{UP} = \sec(\theta) \cdot \int_0^\infty \kappa_\alpha(f,z) \cdot T(z) \cdot e^{-\tau(z,\infty)} \cdot dz, \quad (2)$$

$$T_b = e_s \cdot T_s \cdot e^{-\tau(0,\infty)}, \quad (3)$$

and

$$T_{SC} = (1 - e_s) \cdot \sec(\theta) \cdot \int_\infty^0 \kappa_\alpha(f,z) \cdot T(z) \cdot e^{-\tau(0,z)} dz, \quad (4)$$

where each contribution to the brightness temperature is represented in the Fig. 2:

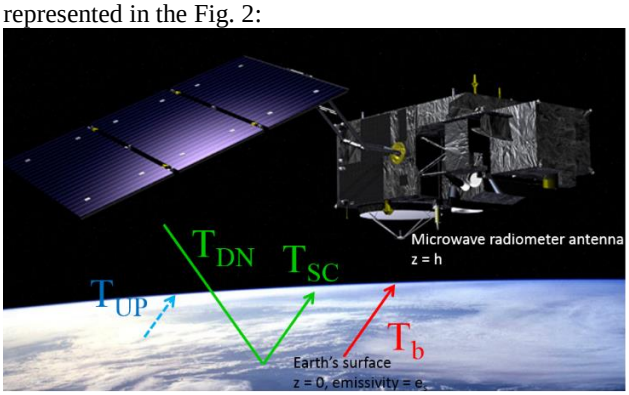

Fig. 2. Schematic observation brightness temperatures.

In Eqns. 3 and 4, e_s and T_s are the surface's emissivity and temperature, and θ is the zenith angle.
The brightness temperature reaching the radiometer (T_B) can also be written as:

$$T_B = \sec(\theta) \cdot \int_0^\infty \rho_v(f,z) \cdot K^\uparrow{}_W(f,\theta,z) \cdot dz, \quad (5)$$

where $K^\uparrow{}_W$ is the so-called water vapor weighting function, which indicates the contribution of the atmospheric water vapor content at height z, to the measured brightness temperature (T_B) at a frequency f, under an observation angle θ ($\theta = 0°$ at nadir) and, over surface with emissivity e_s [3]. The water vapor weighting function is calculated as the derivative of the brightness temperature with respect to the water vapor profile:

$$K^\uparrow{}_W(f,\theta,z) = \frac{\partial \kappa_\alpha(f,T,\rho_v)}{\partial \rho_v} \cdot \sec(\theta) \cdot e^{-\tau(z,h)} \cdot \left\{ -[(1-\epsilon) \cdot T_{DN} + \epsilon \cdot T_s] \cdot e^{-\tau(0,z)} - \int_0^z T(z') \cdot \kappa_\alpha(f,T,\rho_v) \cdot \sec(\theta) \cdot e^{-\tau(z',z)} dz' \right\} + K^\downarrow{}_W(f,\theta,z), \quad (6)$$

where $K^\downarrow{}_W(f,\theta,z)$ is the water vapor weighting function for an upward looking radiometer:

$$K^\downarrow{}_W(f,\theta,z) = \frac{\partial \kappa_\alpha(f,T,\rho_v)}{\partial \rho_v} \cdot \sec(\theta) \cdot e^{-\tau(h,z)} \cdot \left\{ -\int_z^h T(z') \cdot \kappa_\alpha(f,T,\rho_v) \cdot \sec(\theta) \cdot e^{-\tau(z,z')} dz' \right\}. \quad (7)$$

Equation 6 allows to analyze the sensibility of the observation (i.e. frequency channel) to the atmospheric water vapor variations, and the impact of different surfaces (ice, ocean, and coastal) can be evaluated.

2.2. Channel selection based on the amount of information content

The methodology used in this study consists of the analysis of the sensibility to the atmospheric water vapor content of the brightness temperatures measured from the space by down-looking microwave radiometer, and the evaluation of the optimum set of frequency channels that provide the largest amount of information on the water vapor content, i.e. the information provided by the selected channels is most uncorrelated. Once a channel is selected, the information provided is considered to be known at the time to select further channels, i.e. it is no longer a variable, avoiding redundant data.

2.2.1 Information content

To compute the information content of the different frequency channels, the concept of entropy of the probability density functions is used as defined by Shannon

in Information Theory [4, pp. 33-34]. The quantity of information of a given parameter that is provided by some observations (frequency channel) is computed as the change in the information entropy from a prior knowledge state of this parameter, and its knowledge after that observation. This is expressed in Eqns. 8 and 9, where the analyzed state is $\boldsymbol{x}$, the observations are $\boldsymbol{y}$, S indicates the entropy of the state with probability P, and H is the reduction in the entropy or information content.

$$H_n = S[P(\boldsymbol{x})] - S[P(\boldsymbol{x}|\hat{\boldsymbol{y}})]\,, \tag{8}$$

$$H_m = S[P(\hat{\boldsymbol{y}})] - S[P(\hat{\boldsymbol{y}}|\boldsymbol{x})]. \tag{9}$$

In Eqn. 8 the entropy reduction is evaluated in the state space or atmospheric profile, i.e. the change in the entropy of the state vector when it is improved by the measurements, where the subscript n is the number of atmospheric layers. In Eqn. 9 the entropy reduction is evaluated in the measurement space, i.e. the change in the entropy of the measurements when the state space is previously known, where the subscript m is the number of observation channels (or frequencies). The result obtained for each equation is the same, and could be combined to measure the reduction entropy when other channels are previously selected.

2.2.2. Model linearization

The forward model presented in Eqns. 1 and 5 can be discretized in order to facilitate the calculation using algebraic methods [3]. This discrete model is presented below, where the bold symbols indicate vectors (lower case) and matrices (upper case).

$$\hat{\boldsymbol{y}} = \boldsymbol{K_W} \cdot \boldsymbol{x} + \boldsymbol{\varepsilon}. \tag{10}$$

In this discrete model the brightness temperature observations are represented by the vector $\hat{\boldsymbol{y}}$, whose dimension corresponds to the number of observation channels (frequency channels) to be analyzed. The unknown profile information along the atmospheric height z is $\boldsymbol{x}$, the error of each observation caused by the instruments' calibration and the noise is $\boldsymbol{\varepsilon}$, and the contribution of each atmospheric profile component per height and frequency to the brightness temperature is given by the matrix $\boldsymbol{K_W}$. The weighting function matrix $\boldsymbol{K_W}$ is m xn, where there is a contribution to the brightness temperature at each frequency channel (m channels) from each layer (n layers). The number of layers (n) is 60 between 0 and 64 km in steps of 0.1 to 0.8 km for the troposphere, 0.8 to 2 km for the stratosphere and, 2 to 4 km for the mesosphere.The total number of channels (m) around the water vapor resonance frequencies (22.235 GHz and 183.3 GHz) are analyzed in steps of 100 MHz.

The probability density function of the measurements is assumed to be Gaussian function in order to use its properties, and to relate the probability density function of the observations with the one of the atmospheric state (Eqns. 8 and 9), by using Bayes' theorem (Eqns. 11 and 12).

$$P(\hat{\boldsymbol{y}}|\boldsymbol{x}) = P(\boldsymbol{x},\boldsymbol{y}) / \int P(\boldsymbol{x},\hat{\boldsymbol{y}}), \tag{11}$$

$$P(\boldsymbol{x}|\boldsymbol{y}) = P(\hat{\boldsymbol{y}}|\boldsymbol{x}) \cdot P(\boldsymbol{x}) / P(\hat{\boldsymbol{y}}). \tag{12}$$

Assuming $P(\hat{\boldsymbol{y}})$ and $P(\boldsymbol{x})$ are Gaussian functions with a zero-mean experimental error $\boldsymbol{\varepsilon}$, Eqns. 11 and 12 become:

$$P(\boldsymbol{y}) = \frac{1}{(2\pi)^{\frac{n}{2}} \cdot |\boldsymbol{S_y}|^{\frac{1}{2}}} \cdot e^{-\frac{1}{2}\cdot(\boldsymbol{y}-\boldsymbol{E}(\boldsymbol{y}))\cdot \boldsymbol{S_y^{-1}} \cdot (\boldsymbol{y}-\boldsymbol{E}(\boldsymbol{y}))}\,, \tag{13}$$

$$P(\boldsymbol{x}) = \frac{1}{(2\pi)^{\frac{n}{2}} \cdot |\boldsymbol{S_a}|^{\frac{1}{2}}} \cdot e^{-\frac{1}{2}\cdot(\boldsymbol{x}-\boldsymbol{x_a})\cdot \boldsymbol{S_a^{-1}} \cdot (\boldsymbol{x}-\boldsymbol{x_a})}, \tag{14}$$

where the matrices $\boldsymbol{S_y}$ and $\boldsymbol{S_a}$ are the covariance matrices of $\hat{\boldsymbol{y}}$ and $\boldsymbol{x_a}$, respectively, and the subscript a denotes the *a priori* knowledge coming from historical information of the atmosphere or from synthetic data as in the case of this study. By combining Eqns. 13 and 14 [4, pp. 23 – 29], the covariance matrix of the state vector improved by the brightness temperature observations (Eqn. 12) can be written as:

$$\hat{\boldsymbol{S}}^{-1} = \boldsymbol{K_w^T} \cdot \boldsymbol{S_\varepsilon^{-1}} \cdot \boldsymbol{K_W} + \boldsymbol{S_a^{-1}}. \tag{15}$$

From the discretization of the observations and the atmospheric state given by Eqn. 10, and defining the relationship between the *a priori* knowledge of the atmospheric state $\boldsymbol{x}$ with the knowledge gain obtained through the observations (Eqns. 11 and 12), the recovered state vector $\hat{\boldsymbol{x}}$ can be expressed as:

$$\hat{\boldsymbol{x}} = \boldsymbol{x_a} + \boldsymbol{S_a} \cdot \boldsymbol{K_W^T} \cdot \left(\boldsymbol{K_W} \cdot \boldsymbol{S_a} \cdot \boldsymbol{K_W^T} + \boldsymbol{S_\varepsilon}\right)^{-1} \cdot (\hat{\boldsymbol{y}} - \boldsymbol{K_W} \cdot \boldsymbol{x_a}), \tag{16}$$

that can also be rewritten as:

$$\hat{\boldsymbol{x}} = \boldsymbol{x_a} + \boldsymbol{G} \cdot (\hat{\boldsymbol{y}} - \boldsymbol{K_W} \cdot \boldsymbol{x_a}), \tag{17}$$

where $\boldsymbol{G}$ denotes the contribution matrix or gain matrix.
The so-called Averaging Kernel (Eqn. 18):

$$\boldsymbol{AK} = \boldsymbol{S_a} \cdot \boldsymbol{K_W^T} \cdot \left(\boldsymbol{K_W} \cdot \boldsymbol{S_a} \cdot \boldsymbol{K_W^T} + \boldsymbol{S_\varepsilon}\right)^{-1} \cdot \boldsymbol{K_W} \cdot \boldsymbol{S_a} \tag{18}$$

describes the vertical correlation between the parameters at different heights for a given set of frequency channels, and it will be used to measure the entropy reduction by each channel.

2.2.3. Channel Selection Iterative Method

The method used to select the optimum set of frequencies consists of the evaluation of the information content of each individual frequency channel, and taking into account the previously selected ones (Eqns. 8 and 9). The change on the measurement entropy caused by each selected channel is evaluated (Eqn. 9), which at the same time changes the vertical entropy (Eqn. 8). From the linearized model of the previous section (Eqn. 10), the entropy (in bits) of a multivariate Gaussian distribution for a vector can be approximated as:

$$S[P(\boldsymbol{y})] \approx \frac{1}{2}\log_2[S(\boldsymbol{y})], \tag{19}$$

where $S(\boldsymbol{y})$ is the covariance matrix of this vector. Thus, for the discrete model in Eqn. 9 can be expressed as:

$$H_m = \frac{1}{2}\log_2\left[\boldsymbol{I_m} + \boldsymbol{K'_W}\cdot\boldsymbol{A}\cdot\boldsymbol{K'^T_W}\right], \quad (20)$$

where

$$\boldsymbol{K'_W} = \widehat{\boldsymbol{S_\varepsilon}}^{-\frac{1}{2}}\cdot\boldsymbol{K_W}\,, \quad (21)$$

and $\boldsymbol{A}$ indicates the improvement of the different frequencies on the atmospheric profile information or state vector [4, pp. 29 – 33], [5].

From Eqns. 8 and 18, the entropy reduction in the state space can be evaluated as:

$$H_n = -\frac{1}{2}\cdot\log_2[\boldsymbol{I_n} - \boldsymbol{S_a}\cdot\boldsymbol{K_W^T}\cdot\left(\boldsymbol{K_W}\cdot\boldsymbol{S_a}\cdot\boldsymbol{K_W^T} + \boldsymbol{S_\varepsilon}\right)^{-1}\cdot \boldsymbol{K_W}]. \quad (22)$$

and from Eqn. 18, it can be expressed as:

$$H_n = -\frac{1}{2}\cdot\log_2[\boldsymbol{I_n} - \boldsymbol{AK}]. \quad (23)$$

The change in the state space covariance because of the selected channels is:

$$\boldsymbol{A} = \left[\boldsymbol{I_n} - \boldsymbol{S_a}\cdot\boldsymbol{K_W^T}\cdot\left(\boldsymbol{K_W}\cdot\boldsymbol{S_a}\cdot\boldsymbol{K_W^T} + \boldsymbol{S_\varepsilon}\right)^{-1}\cdot\boldsymbol{K_W}\right]\cdot\boldsymbol{S_a}, \quad (24)$$

and from Eqn. 22

$$-\frac{1}{2}\cdot\log_2[\boldsymbol{A}] = H_n + \log_2[\boldsymbol{S_a}]. \quad (25)$$

Finally, Eqn. 20 can be expressed as the entropy in the measurement space of the remaining channels updated by the entropy in the state space for the selected channels:

$$H_m = \frac{1}{2}\log_2\left[\boldsymbol{I_m} + \boldsymbol{K'_W}\cdot H_n\cdot\boldsymbol{S_a}\cdot\boldsymbol{K'^T_W}\right], \quad (26)$$

Using Eqn. 26 iteratively, the information content of channel i (Entropy Reduction or δER_i) can be evaluated separately (Eqn. 27). The one providing the largest amount of information is then kept:

$$\delta ER_i = \frac{1}{2}\log_2[1 + \boldsymbol{k'_{w_i}}\cdot\boldsymbol{A_{i-1}}\cdot\boldsymbol{k'^T}], \quad (27)$$

where $\boldsymbol{A_{i-1}}$ accounts for the channels previously selected.

$$\boldsymbol{A_i} = \boldsymbol{A_{i-1}} - \frac{(\boldsymbol{A_{i-1}}\cdot\boldsymbol{k_{i'}^T})\cdot(\boldsymbol{A_{i-1}}\cdot\boldsymbol{k_{i'}^T})^T}{1+(\boldsymbol{A_{i-1}}\cdot\boldsymbol{k_{i'}^T})^T\cdot\boldsymbol{k_{i'}^T}}, \quad (28)$$

with $\boldsymbol{A_0} \triangleq \boldsymbol{S_a}$.

4. WATER VAPOR RESONANCE FREQUENCIES

The Entropy Reduction method gives a ranking of the most suitable frequencies (channels) to retrieve the atmospheric component of interest, from a spaceborne radiometer. Furthermore, the frequencies are evaluated by considering their contribution in case a set of channels is used for the analysis, i.e. the information provided by a frequency (channel) is uncorrelated to the one provided by the previous selected channel's, in case there is a previous selection iteration. As explained in section 2, the information content of each frequency is measured through the water vapor weighting functions from the down-looking brightness temperature (Eqn. 6), which provides the sensibility of the measured brightness to changes in the atmospheric water vapor profile. This sensibility is evaluated considering the radiation emitted by the atmosphere directly to the downlooking spaceborne radiometer (T_{UP}), the radiation emitted by the atmosphere down to the surface (T_{SC}) and reflected back to the space radiometer (T_{DN}), and the radiation emitted by the Earth surface (T_B). The atmospheric radiation emitted to the space, gives the trend of the water vapor with regards to the climate, however, it does not provide information on the impact of the surface change on the variability of the atmospheric water vapor content. Water vapor profile changes caused by the surface characteristics, are a case of interest for this study to correct the electrical path wet delay on coastal altimeters, as its rapid variability is one of the main reasons that makes this information inaccurate. The information on the effect of the surface into the atmospheric state is given by the reflected downwelling temperature, and by the surface emitted temperature, which are directly related to the surface emissivity.

Temperate and tropical climates are wetter than polar climate, which is practically dry. It causes that around the water vapor absorption window around 183.31 GHz, the oblique transmissivity for temperate and tropical climates is zero (opaque atmosphere), while in polar climates is between 20-30%. This fact affects to the depth along the atmosphere to which the radiometers can measure the water vapor content in temperate and tropical climates, making frequencies around 183.3 GHz not suitable for surface water vapor variability studies, being necessary to move to the tails of this resonance frequency to better analyze the sensitivity to the water vapor [6]. On the other hand, in the low water vapor absorption window, around 22.23 GHz, the oblique transmissivity is higher for the three climates (ratio between 85-95% in tropical and temperate climates, and ~100% in polar climates), making it possible to analyze the surface emissivity effects on the water vapor variability of the low-troposphere. On the other hand, due to the fact that the water absorption lines are stronger at the higher resonance frequencies (183.31 GHz), the information content provided in these frequencies would be always larger than the one provided by the lower frequencies (22.23 GHz). However, the information content measured in the 183.31 GHz window in temperate and tropical climates will be coming from the mid-low troposphere. Therefore it is necessary to analyze both absorption windows separately, and from the two remaining set of frequencies, select those ones that include information along all the mid-lower troposphere.

3. SIMULATION RESULTS

In a preliminary study all the frequency channels from 1 to 200 GHz were studied, considering only the contribution of the atmospheric water vapor to the upwelling brightness temperature (T_{UP}). Results confirmed the intuition, that the best bands are around the lower (~22 GHz), and higher (~183 GHz) water vapor resonance frequencies. Therefore, only the meaningful results for these frequency bands are presented here.

Figures 3 and 4 show the application of the iterative method to the different resonance frequencies, that is the δER_i for the channels that provide the largest amount of information. This is done for the three climates: temperate, tropical and polar, and for the three surfaces: sea, coast, and ice. In these figures, the first iteration of the method (when the first channel is selected) is shown, and then the following iterations, until a significant number of bits of information it is retained, that in this study the threshold is above 0.2 bits of information. Figure 3shows the δER_i for the low (~22 GHz) band and for three different surface emissivities. As mentioned in the previous section, resonance frequencies do not turn to be the optimum ones to retrieve information about the state of the atmosphere, as they are strongly affected by the attenuation. In these figures it can be observed that the trend of the information provided does not vary, that means that the optimum frequencies do not change. However, for increasing surface emissivity (from sea e_s~0.50 to ice e_s~1.00), the information provided by the optimum frequencies also increases. It means that the information given by the surface temperature emitted to the space contains more information about the water vapor

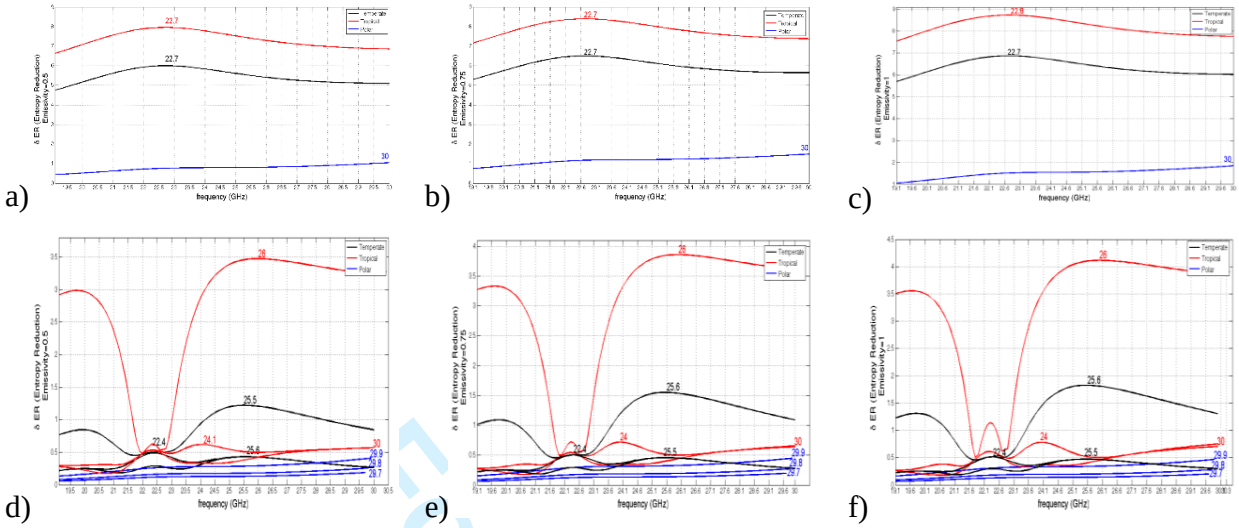

Fig. 3. Entropy Reduction for low frequency channels, for different climates (black: temperate, red: tropical, blue: polar), and different surface emissivities (a-d: e_s=0.50; b-e: e_s=0.75, e_s=1.00). Top row: Entropy reduction when fist channel is selected. Bottom row: Entropy reduction when second, third and fourth channels are selected.

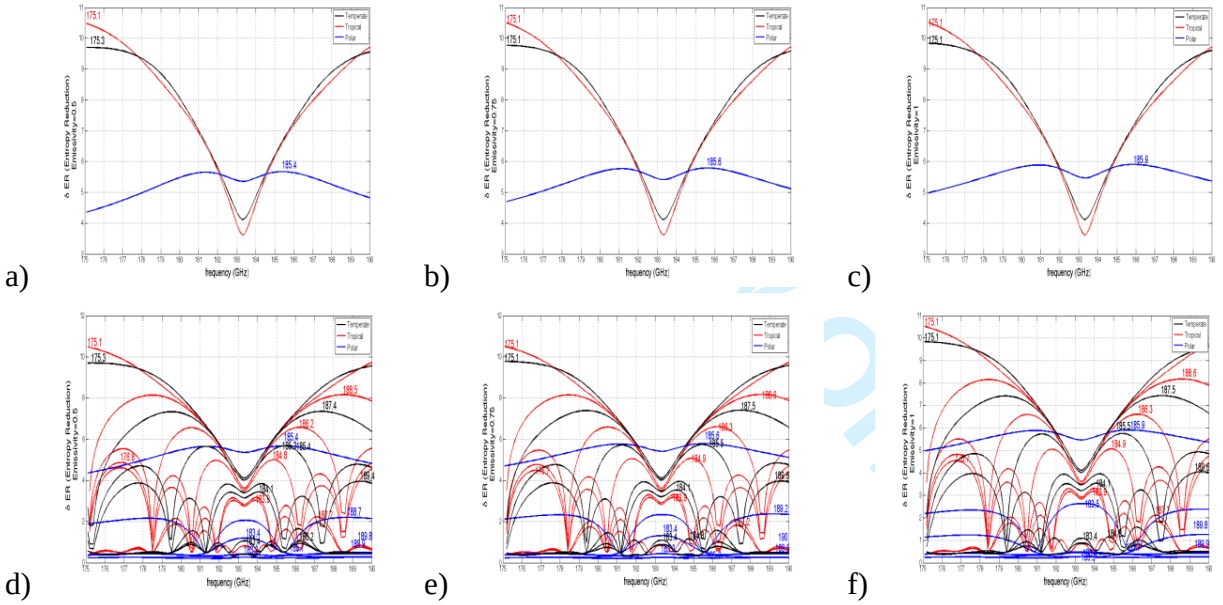

Fig. 4. Entropy Reduction for high frequency channels, for different climates (black: temperate, red: tropical, blue: polar), and different surface emissivities (a-d: e_s=0.50; b-e: e_s=0.75, e_s=1.00). Top row: Entropy reduction when fist channel is selected. Bottom row: Entropy reduction when second to sixth channels are selected.

distribution in the atmosphere than the reflected downwelling temperature. This is due to the fact that as the upwelling temperature, the downwelling temperature corresponds to the radiation emitted by the atmosphere, so it is expected that the information provided is somewhat similar to the one provided by the upwelling temperature. In other words, the information is correlated. At lower frequencies, the information provided by the main channels decays rapidly, i.e. one channel provides almost all the information. This fact indicates that the water vapor information provided by lower the frequency channels is less impacted by the atmosphere gas absorption which is highly correlated, and practically one channel provides most of the information.

Higher resonant frequencies (Fig. 4) provide actually the largest amount of information on the water vapor for the three climates analyzed. In all cases, the main channels correspond to the three first channels of the higher

frequencies. As in case of the lower resonance frequencies, the tails of the sounding channels are best suited to obtain more information, as there is less affectation of the gas absorption.

At both high and low resonance frequencies, the distribution of the information between the remaining channels has a common behavior when a channel is selected. Each time a channel is selected. the information of the remaining channels is reevaluated. discarding those channels that provide information correlated to the information already provided with the selected ones. Since the main channels are at the tails of the resonance frequencies. it can be observed that after the 3th or 4th iteration. the channels containing most information start getting closer to the resonant frequencies. This indicates that the tails are less attenuated. but more correlated among them in terms of amount of information. This effect is clearly visible for the high resonance frequencies in tropical climates. Tables 1–3 show in detail these results numerically.

Table 1. Entropy reduction for low and high frequency channels: temperate climate.

Surface's emissivity e_s=0.50		Surface's emissivity e_s=0.75		Surface's emissivity e_s=1.00	
f [GHz]	ER [bits]	f [GHz]	ER [bits]	f [GHz]	ER [bits]
22.7	6.001	22.7	6.498	22.7	6.868
25.5	1.220	25.6	1.550	25.6	1.824
22.4	0.486	22.4	0.503	22.4	0.513
25.6	0.429	25.5	0.456	25.5	0.471
22.5	0.286	22.3	0.292	22.3	0.296
25.7	0.267	25.7	0.277	25.7	0.282
22.3	0.204	22.5	0.207	22.5	0.208
175.3	9.700	175.1	9.769	175.1	9.837
187.4	7.349	187.5	7.405	187.5	7.437
185.4	5.672	185.5	5.735	185.5	5.751
189.4	3.952	189.6	3.964	189.6	4.050
184.1	3.435	184.1	3.531	184.1	3.535
183.4	1.054	184.8	1.158	184.8	1.162
186.2	0.935	183.4	0.877	183.4	0.877

Table 2. Entropy reduction for low and high frequency channels: tropical climate.

Surface's emissivity e_s=0.50		Surface's emissivity e_s=0.75		Surface's emissivity e_s=1.00	
f [GHz]	ER [bits]	f [GHz]	ER [bits]	f [GHz]	ER [bits]
22.7	7.957	22.7	8.395	22.8	8.732
26.0	3.474	26.0	3.858	26.0	4.115
24.1	0.618	24.0	0.716	24.0	0.779
30.0	0.567	30.0	0.639	30.0	0.704
22.3	0.526	22.3	0.537	22.3	0.595
24.2	0.326	24.2	0.351	24.2	0.361
29.9	0.312	29.9	0.331	29.9	0.344
175.1	10.480	175.1	10.496	175.1	10.511
188.5	8.158	188.6	8.166	188.6	8.174
186.2	6.573	186.3	6.607	186.3	6.611
184.8	4.993	184.9	5.069	184.9	5.071
176.8	4.609	176.7	4.489	176.7	4.544
183.9	3.037	183.9	3.177	183.9	3.179
187.2	1.937	187.2	1.823	187.2	1.838

Table 3. Entropy reduction for low and high frequency channels: polar climate.

Surface's emissivity e_s=0.50		Surface's emissivity e_s=0.75		Surface's emissivity e_s=1.00	
f [GHz]	ER [bits]	f [GHz]	ER [bits]	f [GHz]	ER [bits]
30.0	1.047	30.0	1.491	30.0	1.844
29.9	0.405	29.9	0.448	29.9	0.467
29.8	0.255	29.8	0.271	29.8	0.278
185.4	5.670	185.6	5.787	185.9	5.905
188.7	2.198	189.2	2.366	183.5	2.631
183.4	1.190	183.4	1.315	189.8	1.258

Finally, Fig. 5 presents the weighting functions for the main frequency channels of each climate and surface emissivity. As it can be seen, the first four channels contain information on the water vapor in the troposphere up to ~5-7 km for temperate and tropical climates, and up to ~3-4 km for polar climates. These figures give also a clear view of the impact of the surface emissivity on the sensibility of the brightness temperature to the atmospheric water vapor. As previously discussed, the increase of the surface emissivity augments the presence of the surface temperature into the observations that contains important information on the variability of the water vapor in lower layers of the troposphere, and it is more uncorrelated to the upwelling brightness temperature than the reflected downwelling brightness temperature. This effect can be observed through the polar climates, where there is lower concentration of water vapor in the troposphere. In Figs. 5g-h it can be observed that a frequency channel at 183.4 GHz provides the largest information from the lower troposphere when the surface emissivity is increased. This fact enhances the presence of the surface temperature (T_b) into the retrieved brightness temperature (T_B), that as explained previously is less correlated with the atmospheric radiated temperatures (T_{DN}, and T_{UP}), so that provides more information about the water vapor distribution.

4. CONCLUSIONS AND FUTURE RESEARCH LINES

It has been found that just four frequency channels convey the largest amount of information for all three climates, and information provided by further channels provide at least 4 bits less of information than the previous selected ones.

In higher resonance frequencies the channels that provide the most information are 175.1 GHz, ~188.1 GHz, and ~185.5 GHz for temperate climates, 175.1 GHz, ~188.5 GHz, and ~186.3 GHz for tropical climates and ~185.5 GHz, 189.2 GHz, and 183.5 GHz for polar climates, while in lower absorption bands the optimum channels are: 22.7 GHz, and 25.5 GHz for the temperate climates, 22.7 GHz, and 26 GHz, and around 30 GHz for polar climates. These frequency channels are quite similar for tropical and

temperate climates, but differ from those at polar climates. The number of channels to be included in a radiometer instrument will be ultimately dictated by: 1) the achievable accuracy of the water vapor correction for a given number of frequency channels and associated radiometric errors (both radiometric accuracy or

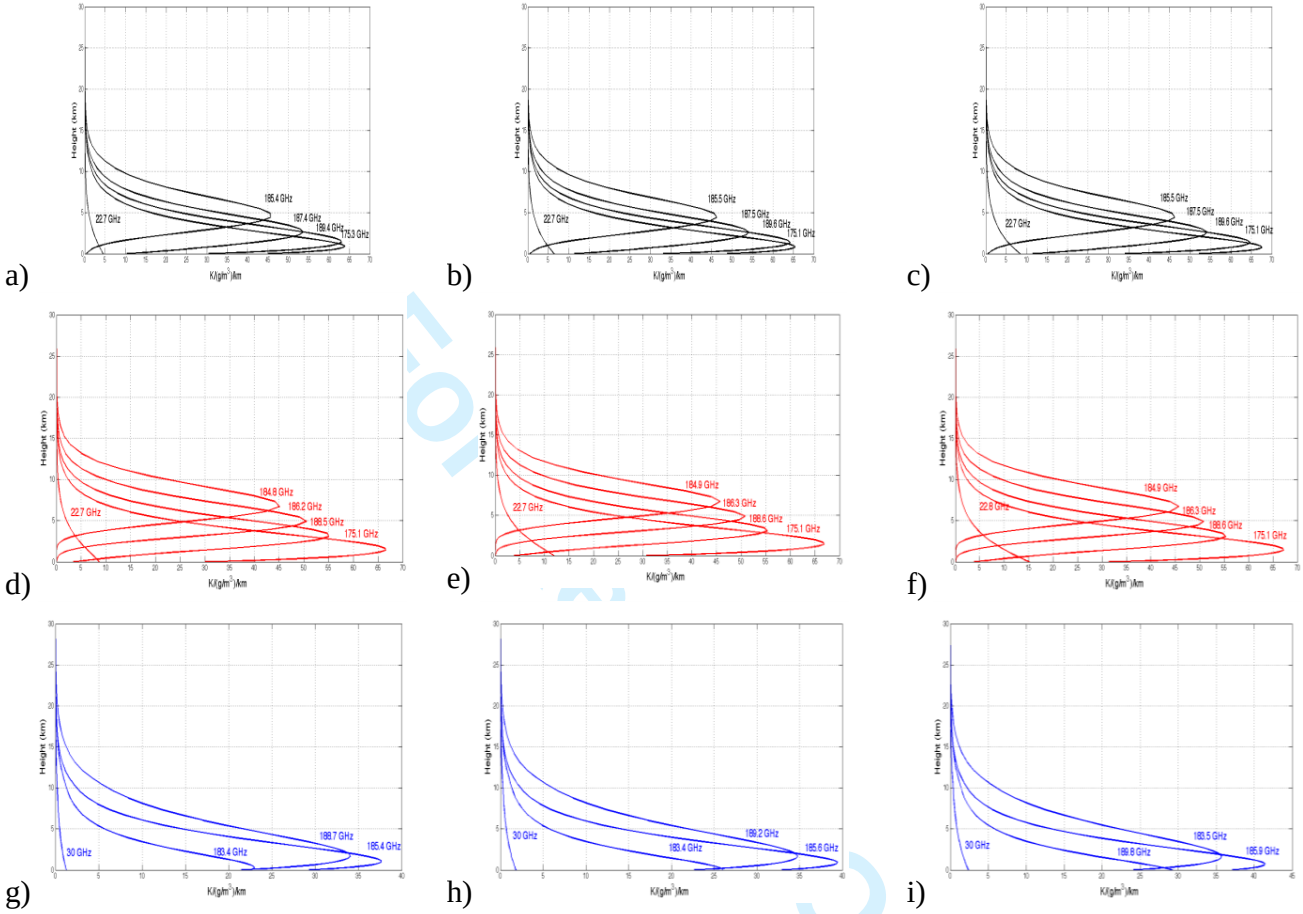

Fig. 5. Weighting functions for: a-b-c) temperate, d-e-f) tropical, and g-h-i) polar climates for the least correlated frequency channels over different surface emissivities: a-d-g) e_s=0.50; b-e-h) e_s=0.75; and c-f-i) e_s=1.00.

systematic errors, and radiometric sensitivity of random errors), and 2) the instrument complexity and cost.

On the other hand, channels of lower resonance frequencies are more sensitive to changes in the surface's emissivity must be included, as they are very sensitive to the variability of water vapor in coastal zones.

Although, a much better spatial resolution can be achieved using the higher frequency channels, as compared to the low frequency channels, for the same antenna size.

Future research lines of this study will extend the range of frequencies (f>200GHz), will consider the atmospheric scattering by hydrometeors, and will perform a study of the achievable wet delay retrieval accuracy as a function of the number of channels and their radiometric errors.

5. REFERENCES

[1] Paolo Cipollini et al., *Product Data Handbook: Coastal Altimetry*. University College Cork: Coastal & Marine Research Centre, ch. 1, pp. 9 – 14.

[2] F.T Ulaby and D.G Long, *Microwave Radar and Radiometric Remote Sensing*. USA: The University of Michigan Press, ch. 8-9, pp. 326-373.

[3] Albin J. Gasiewski, "Nadir sensitivity of passive millimeter and submillimeter wave channels to clear air temperature and water vapor variations", *Journal of Geopyisical Research*, vol. 105, no. D13, pp. 17481 – 17511, July, 2000

[4] C.D Rodgers, *Inverse Methods for atmospheric remote sounding: Theory and Practice*, USA: World Scientific Publishing Co. Pte. Ldt., ch. 2, pp. 20 – 37.

[5] F. Rabier et al., "Channel selection methods for Infrared Atmospheric Sounding Interferometer radiances", *Q. J. R. Meteorol. Soc*, vol. 128, pp. 1011 – 1027, September, 2001.

[6] Dudley B. Chelton et al., *Satellite Altimetry and Earth Sciences*, France: Academic Press, ch. 2, pp. 4 – 11.

AKNOWLEDGEMENTS

This project has received funding by the Spanish Ministry of Economy and Competitiveness ESP2015-70014-C2-1-R (MINECO/FEDER).

BIBLIOGRAPHY

[1] P. R. e. a. Paolo Cipollini, *3rd ESA advanced training on ocean remote sensing*. EESA, 2013. (document), 1.1, 1.1, 1.3

[2] P. C. et al., *Coastal Altimetry Data Handbook*. Coastal & Marine Research Center, 2014. (document), 1, 1.1, 1.2, 1.2.1, 1.2.2

[3] R. K. Raney, "Cryosat sar-mode looks revisited," *IEEE GEOSCIENCE AND REMOTE SENSING LETTERS*, vol. 9, pp. 393 –397, May 2012. 1

[4] P. Cipollini, *Satellite Altimetry and recent advances towards the coast*. National Oceanography Centre, 2010. 1.1

[5] F. M. et al., *Coastal and Hydrology Altimetry product (PISTACH) handbook*. Centre National d'études spatiales, 2010. 1.2.1

[6] A. J. Gasiewski, "Nadir sensitivity of passive millimeter and submillimeter wave channels to clear air temperature and water vapor variations," *Journal of Geophysical Research*, vol. 105, pp. 17 481 –17 511, July 2000. 2, 2.1

[7] C. D. Rodgers, *Inverse methods for atmospheric remote sounding: Theory and Practice*. World Scientific Publishing Co. Pte. Ldt., 2000. 2, 2.2, 2.3.2, 2.3.3

[8] F. T. Ulaby and D. G. Long, *Microwave Radar and Radiometric Remote Sensing*. The University of Michigan press, 2014. 2.1

[9] S. D. M. et al., *Passive Microwave Radiometer Channel Selection Based on Cloud and Precipitation Information Content Estimation*. ECMWF Technical Memoranda, 2005. 2.3.3